ARTERIAL PRESSURE-VOLUME RELATION AND AUGMENTATION INDEX

by

RONALD ANDRE PITT

A thesis submitted to the

Graduate School-New Brunswick

Rutgers, The State University of New Jersey

and

The Graduate School of Biomedical Sciences

UMDNJ- Robert Wood Johnson Medical School

in partial fulfillment of the requirements

for the degree of

Master of Science

Graduate Program in Biomedical Engineering

written under the direction of

Dr. John K-J. Li

and approved by

_____

_____

_____

New Brunswick, New Jersey

January, 2009.

ABSTRACT OF THE THESIS

Arterial Pressure-Volume Relation and Augmentation Index

by **RONALD ANDRE PITT**

Thesis Director:

Dr. John K-J. Li

Hypertension is the primary precursor to all forms of heart disease which according to the CDC continues to be the leading cause of death in the USA. A strong correlation between arterial stiffness and hypertension has been established. Similarly, a decrease in arterial compliance has been shown to be a major causative factor associated with hypertension. Consequently, many studies are designed to identify markers of the health of the arterial system. These markers have not been adequately defined.

To identify possible markers for quantifying arterial properties in hypertension, this thesis evaluates several popular methods for aortic compliance determination from measured aortic pressure and flow waveforms, and then establishes arterial pressure-volume relations as well as proposing new augmentation indices and comparing them with existing ones.

Simultaneously measured aortic pressure and flow waveforms were obtained from experiments performed on anesthetized mongrel dogs during control, methoxamine-induced hypertension and nitroprusside-induced vasodilation. Digitized data sets were

analyzed based on hemodynamic equations established for arterial pressure-volume relation, arterial compliance and augmentation indices.

Results obtained highlighted the consistency in accuracy of the pressure-dependent compliance in predicting the aortic blood pressure. The average gradient of the volume-pressure decreased under hypertensive conditions indicative of the decreased compliance. The comparison of augmentation indices revealed that the most popular method actually produced the least significant distinction between the three conditions. However, all methods produced satisfactory ANOVA results ($P < 0.001$) for separation of means in differentiating control from hypertension and subsequent vasodilation.

Acknowledgements

Firstly, I wish to thank my advisor, Dr. John K-J Li, for his guidance and steadfast support. Without his efforts and patience this thesis would not be completed.

I also acknowledge the tremendous contributions of my parents, Dr. James S.D. Pitt and Valeria E. Pitt, and my loving wife, Dr. Shawna C. Pitt. Thank you all for your unconditional support and prayers.

Table of Contents

List of tables

List of illustrations

Chapter 1. Introduction

1.1 Anatomy of the Arterial System

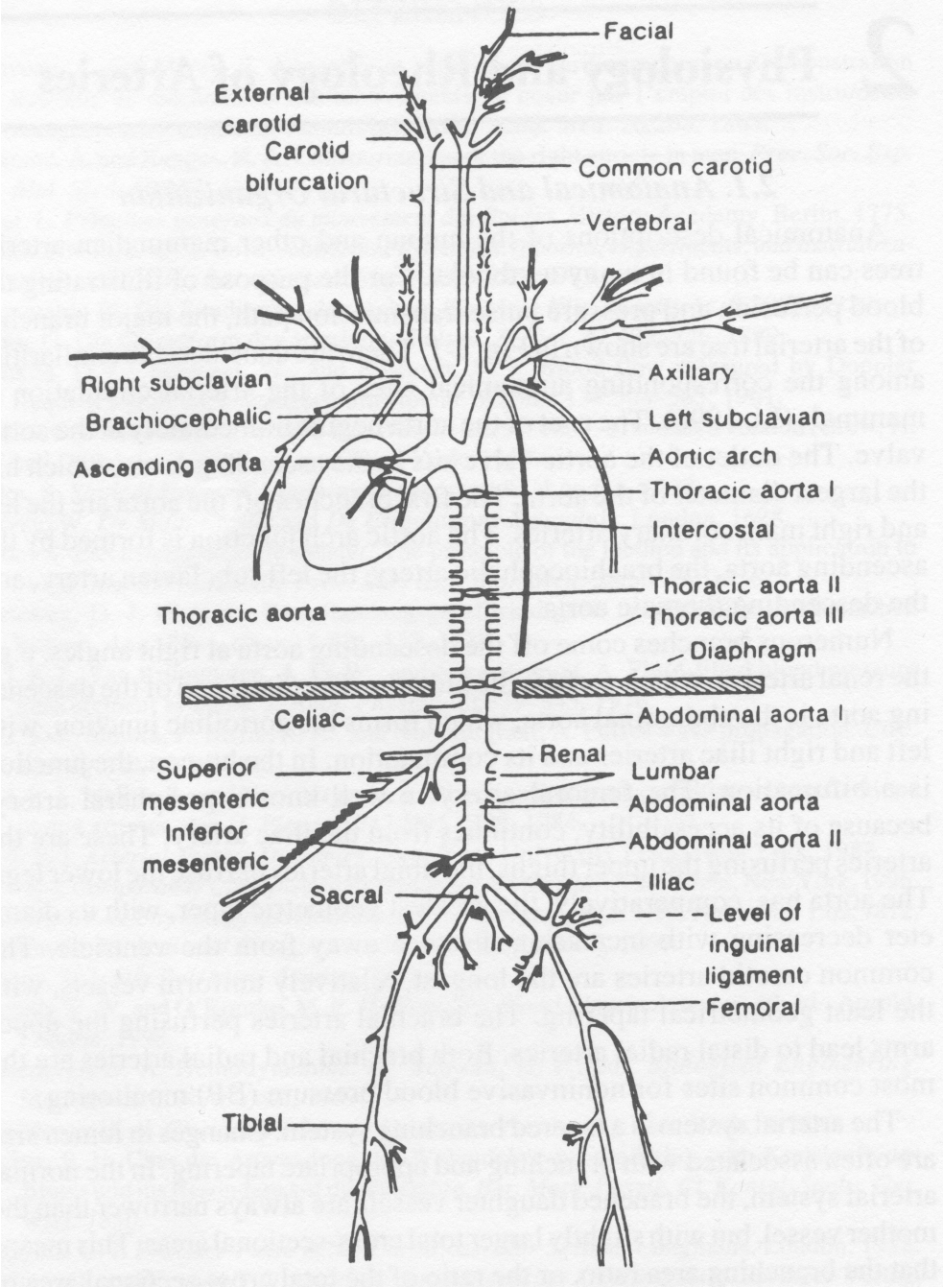

Figure 1.1 - Schematic drawing of arterial tree of a dog showing geometric tapering and branching characteristics of arterial system. From Li (2004)

The arterial system references the network of blood vessels that carry oxygenated blood away from the heart to organs. The arterial system is branched beginning with the ascending aorta. Most of the branches are asymmetrical bifurcations; however, higher order branching also occurs. Figure 1.1 illustrates the layout of arteries in a dog. The structure in man and in several other mammals can be expected to be quite similar. Many mammalian species demonstrate similar pressure and flow waveforms at respective sites along the arterial tree (Li, 1996). As such, inferences about the human arterial system can be drawn from experiments on other mammalian species, especially those of comparable weight and size.

In this thesis the experiments were carried out on 20 to 24 kg dogs, mammals approximately one third the weight of an average human. The drawing shows the decrease in diameter of the arteries as they progress to the periphery. Diameter changes also occur at the branches, with the daughter branches having smaller diameters than the parent. However in general the sum of the cross-sectional area of the daughters is larger than the cross-sectional area of the parent artery. The descending aorta is also clearly tapered, narrowing as it extends away from the heart.

Figure 1.2 illustrates the human arterial system. The similarities to that of the canine system can be seen by comparing Figures 1.1 and 1.2. The branching arrangement is quite similar, thus it can be assumed that experimental conclusions from canines can be extended to human physiology. This assertion is supported by experiments done on mammalian allometry (Stahl, 1963, 1965; Holt et al., 1968, 1981; Calder, 1981, 1996; Li, 1998).

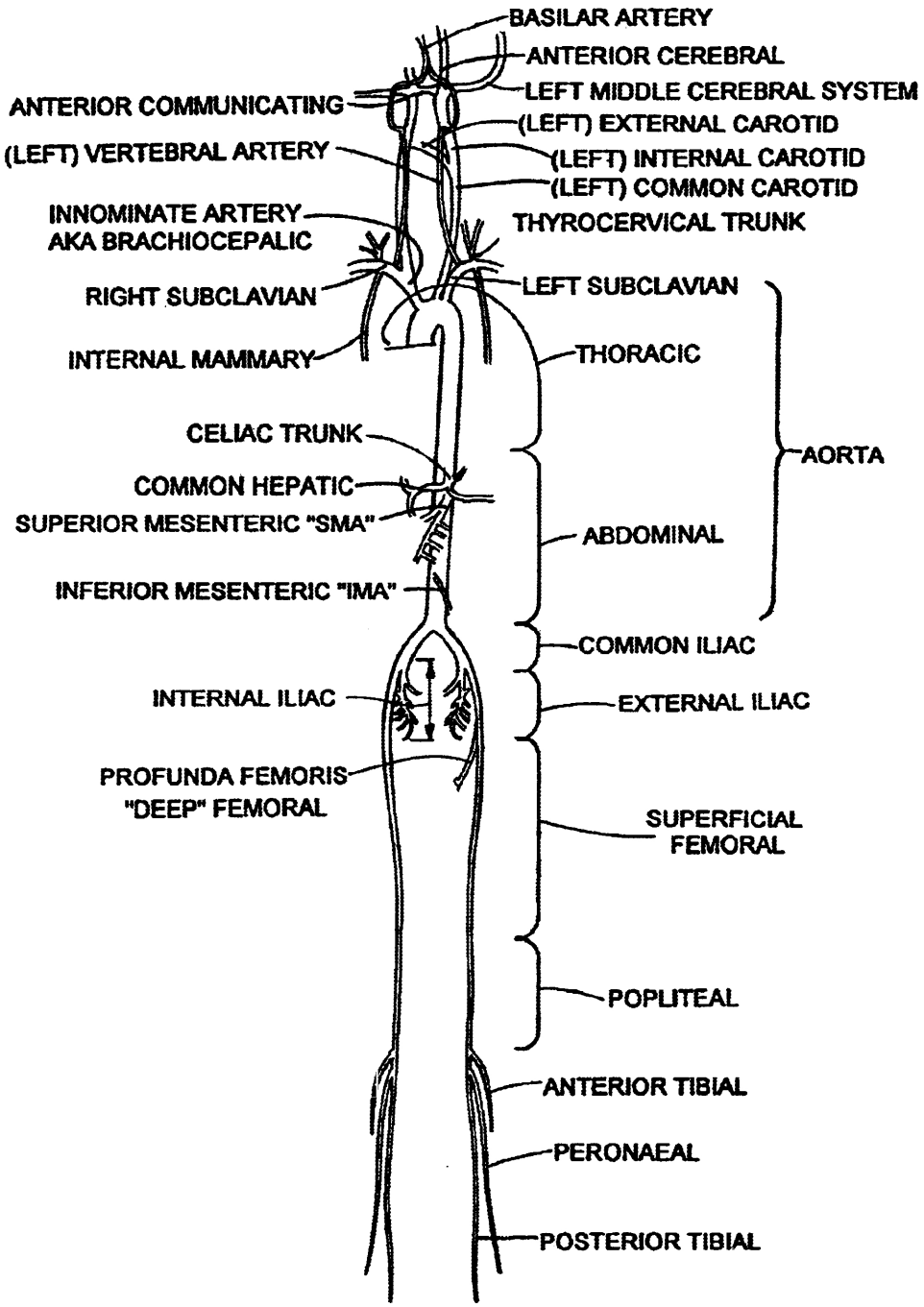

Figure 1.2 - Drawing of human arterial tree. (Garrett Jr. et al 2004)

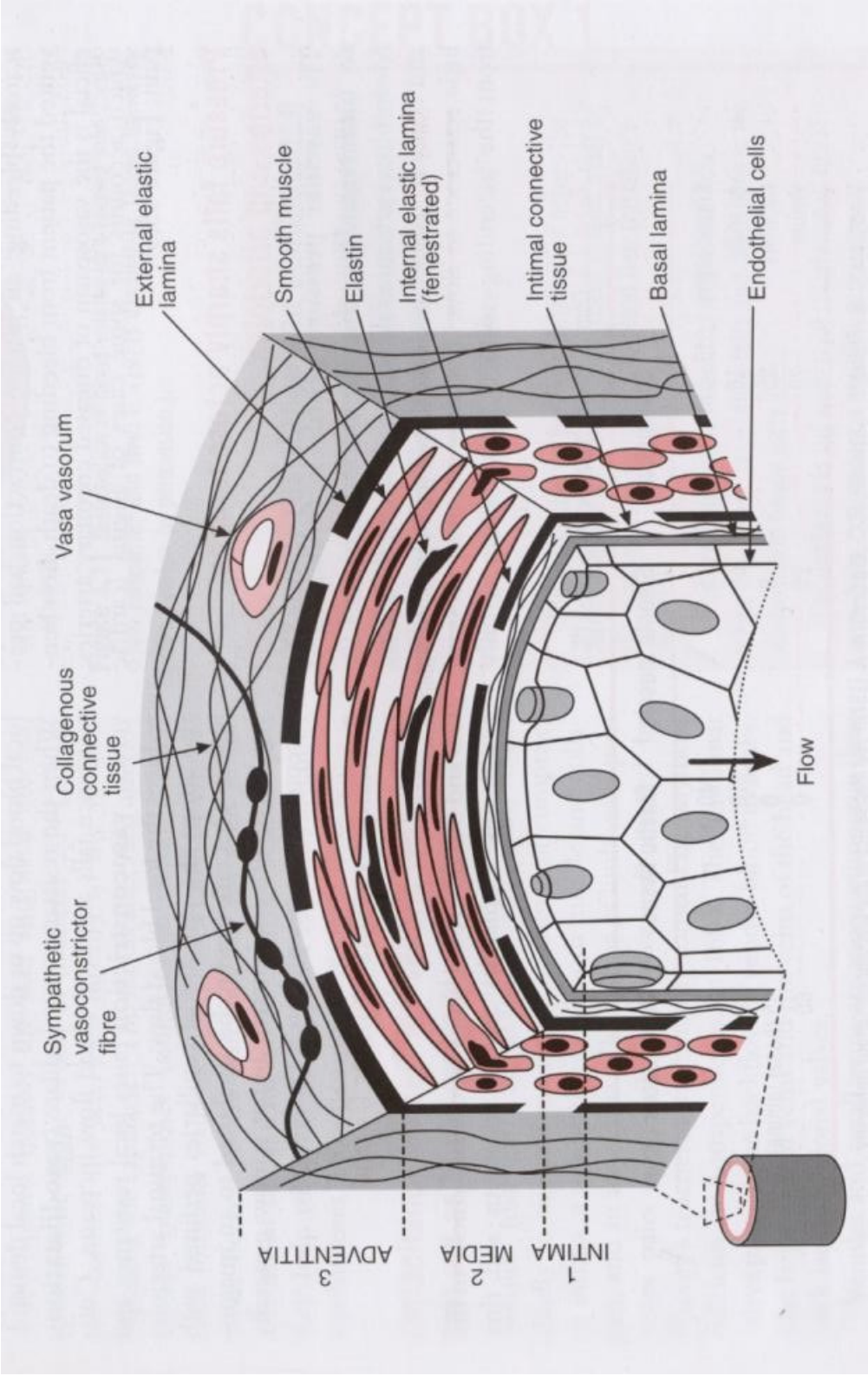

Figure 1.3 - Section of the wall of a typical artery

A cross sectional view of a typical artery, as shown in Figure 1.3 on previous page, reveals three primary layers, the intima, media and adventitia, laminating two elastin rich layers. The layers, in order of innermost to outermost, are:

1. Tunica **intima** - comprised of the single-cell endothelium supported by an elastin and collagen basement membrane (basal lamina). This layer provides the barrier to the blood and also produces and secretes vasoactive chemicals.
2. Internal elastic lamina – single layer of elastic tissue comprising part of basal lamina.
3. Tunica **media** – here smooth muscle cells are arranged in concentric circles around the lumen of the vessel, intermingled with elastin and collagen fibers. This arrangement provides contractility and mechanical strength.
4. External elastic lamina – single layer of elastic tissue
5. Tunica **adventitia** – layer of elastin and collagen fibers that secure the artery to the surrounding tissue. This layer also contains the "vessels of the vessels", vasa vasorum. These local capillaries facilitate metabolite exchange for cells within the thick arterial walls.

Elastin, an elastic protein that is comprised mainly of the amino acids glycine, valine, alanine and proline, is present in all layers throughout the arterial wall. This results in the high elasticity observed in arteries. The collagen present provides structural support, keeping the vessel open in a stent-like manner, but ultimately limiting the extensibility of the blood vessel. Smooth muscles allow for control of the arterial tone through sympathetic and parasympathetic innervation.

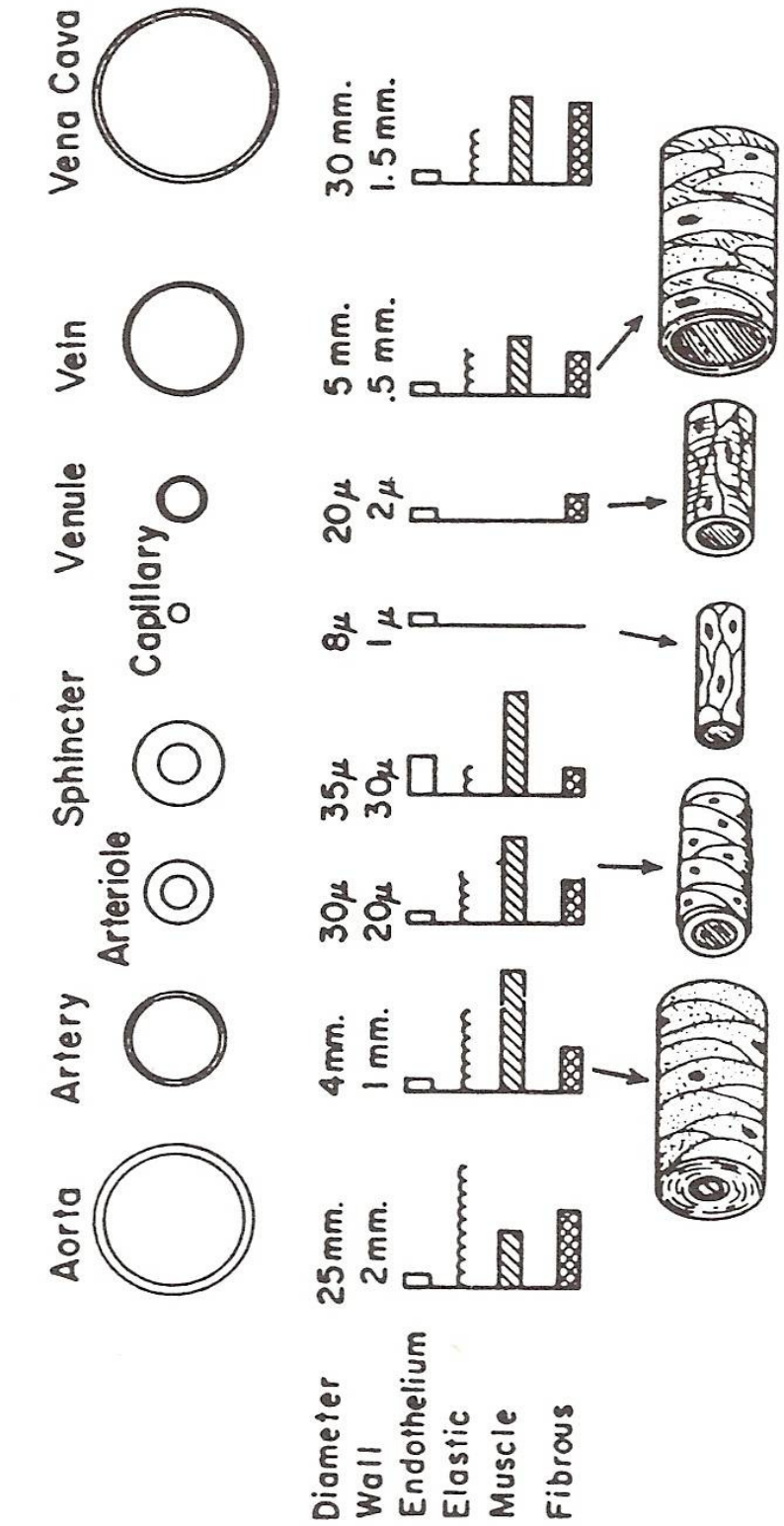

Figure 1.4 - Comparison of the relative content of different vessels in circulatory system. From Li (2004).

Figure 1.4 above further highlights the elasticity of the arterial vessels especially when compared to their corresponding venous vessels. Also important to note is the high muscle content of the arteries and arterioles. (Sphincter in figure 1.4 references the terminal arterioles that contain pre-capillary sphincter muscles allowing control of blood flow to specific capillary beds).

1.2 Cardiovascular Physiology

Blood flow in mammals is fueled by the rhythmic contraction of the heart. This cyclic contraction is comprised of two primary phases – systole and diastole. During systole, the ventricles contract while the atria relax and fill with returning blood. And during diastole the atria contract forcing blood into the now relaxed ventricles. The human heart repeats these events approximately every second. The regulation of the cardiac cycle is achieved in three fundamental ways – mechanically, electrically and chemically.

1.2.1 Mechanical Control

Commonly referred to as the Frank-Starling Mechanism, this means of control is based on the intrinsic property of striated muscle to contract with increased force in response to being stretched within a certain extent. As such, the heart, when faced with increased venous return, contracts more forcibly and completely resulting in an increased stroke volume to match the venous return.

1.2.2 Electrical control (Nervous Control)

The heart is innervated by both sides of the autonomous nervous system (ANS) - the sympathetic and parasympathetic nerves (vagus nerves). Sympathetic stimulation along with parasympathetic inhibition causes an increase in cardiac output, and conversely, output decreases with parasympathetic stimulation and sympathetic inhibition. Thus the ANS provides beat to beat control of the heart. This regulatory aspect comprises the basis for the ubiquitous electrocardiogram (EKG). Under normal conditions the heart is paced by the self-excitatory sinoatrial (SA) node. The action potential generated spreads through the atria, the distribution being aided by the presence of internodal pathways, so called since they ultimately connect to the atrioventricular (AV) node. Figure 1.5 illustrates the cardiac innervation and effects sympathetic and parasympathetic stimuli.

1.2.3 Chemical (Endocrine) control

This control pathway allows for the slow averaged pacing of the heart in relations to other physiological systems. Chemicals that affect how fast the heart beats are said to have chronotropic effects, whereas chemicals which affect contractility of the heart are said to have inotropic effects. Regulation of these various chemicals enables communication of the various organ systems leading to homeostasis.

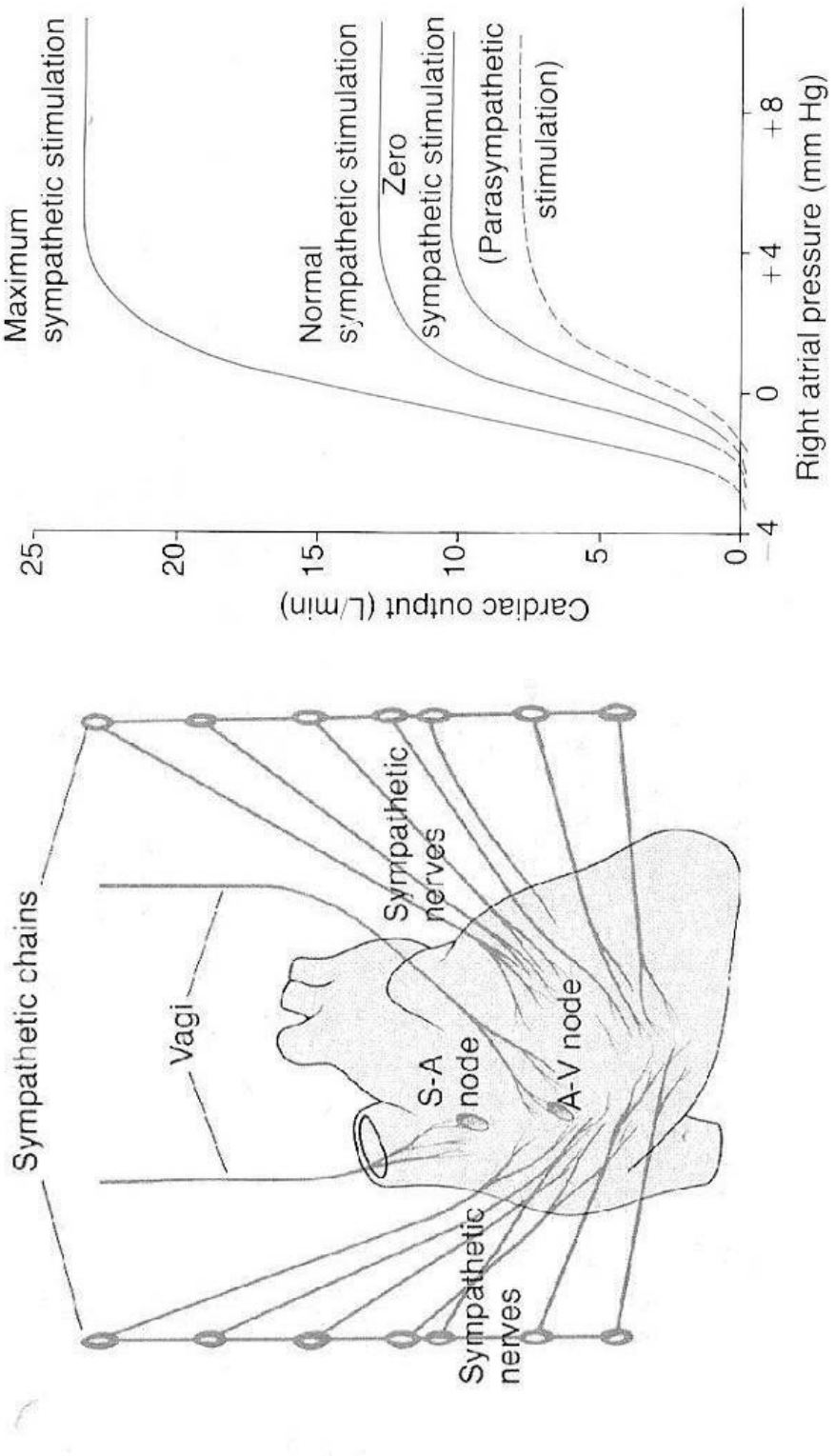

Figure 1.5 - Drawing of cardiac nerves and effect of stimulation on cardiac output. Adapted from Guyton 1991.

1.3 Flow Impedance of Arteries

1.3.1 Resistance

Being tubes, the basic laws of physics tell us that all blood vessels would be resistant to flow. Of course the arteries are no exception and contribute to the peripheral resistance of the cardiovascular system. From Hagen-Poiseuille's law we know that if radius is halved then resistance to flow is increased sixteen-fold. Thus, the arterioles are the primary contributors to overall resistance of the arterial system. The total peripheral resistance indicates the frequency independent opposition by the vasculature to blood flow. This component is physiological mediated by the constriction and dilation of the terminal arterioles. Resistance is derived simply as the ratio of the mean arterial pressure to mean flow through the arteries.

1.3.2 Compliance

The elasticity of the artery wall bestows upon it the property of compliance. Compliance is defined as change in volume per unit change in pressure. As such, it may be viewed as three-dimensional elasticity – example a balloon as a collective unit (3D), compared to a length of balloon material (linear). Though not highly compliant, the arteries are sufficiently compliant to add further intrigue to the puzzle of cardiovascular system dynamics. Research has shown that the arterial compliance varies with pressure. As the pressure increases the compliance decreases exponentially. Over the range of typical physiological pressures, the compliance change is small. However, this non-linearity of the arterial compliance further complicates the modeling of the

cardiovascular system. While some researchers treat the compliance as being linear, Li *et al.* (1994) showed that a nonlinear compliance within the 3-element windkessel model more accurately predicts the aortic pressure waveform.

Linear compliance can be derived by other experimental methods. One method uses pressure decay time constant analogous to the voltage decay time constant of a capacitor. Another method estimates the compliance as the ratio of the stroke volume to pulse pressure (peak systolic – end-diastolic pressure)

$$(1.1) \quad C = \frac{dV}{dP} = ae^{-bP}$$

The constant, *a,* was obtained from previous reports (Li et al. 1986; Wang et al 1986), where curve-fitting of experimentally measured aortic pressure and diameter was used to derive *a* and *b*. The constant b was then calculated by assuming the compliance at mean aortic pressure is equal to the compliance as determined by the time-domain method (Equation 1.2 below).

$$(1.2) \quad C_t = \frac{-t_d}{R_s \ln\left(\frac{P_{ed}}{P_{es}}\right)}$$

$$(1.3) \quad C_V = \frac{SV}{PP}$$

where, (1.4) $$SV = \int_0^T Q_{ao}(t)dt$$

and, (1.5) $$PP = P_{\max} - P_{es}$$

The area method (Liu et al 1986), which uses the area under the systolic and diastolic regions of the aortic pressure wave to estimate the total arterial compliance, was not used.

1.3.3 Inertance

Simply represents the mass of the blood in the system. Like all real masses Newton's second law of motion would apply – an external force is required to alter the state of motion of the mass.

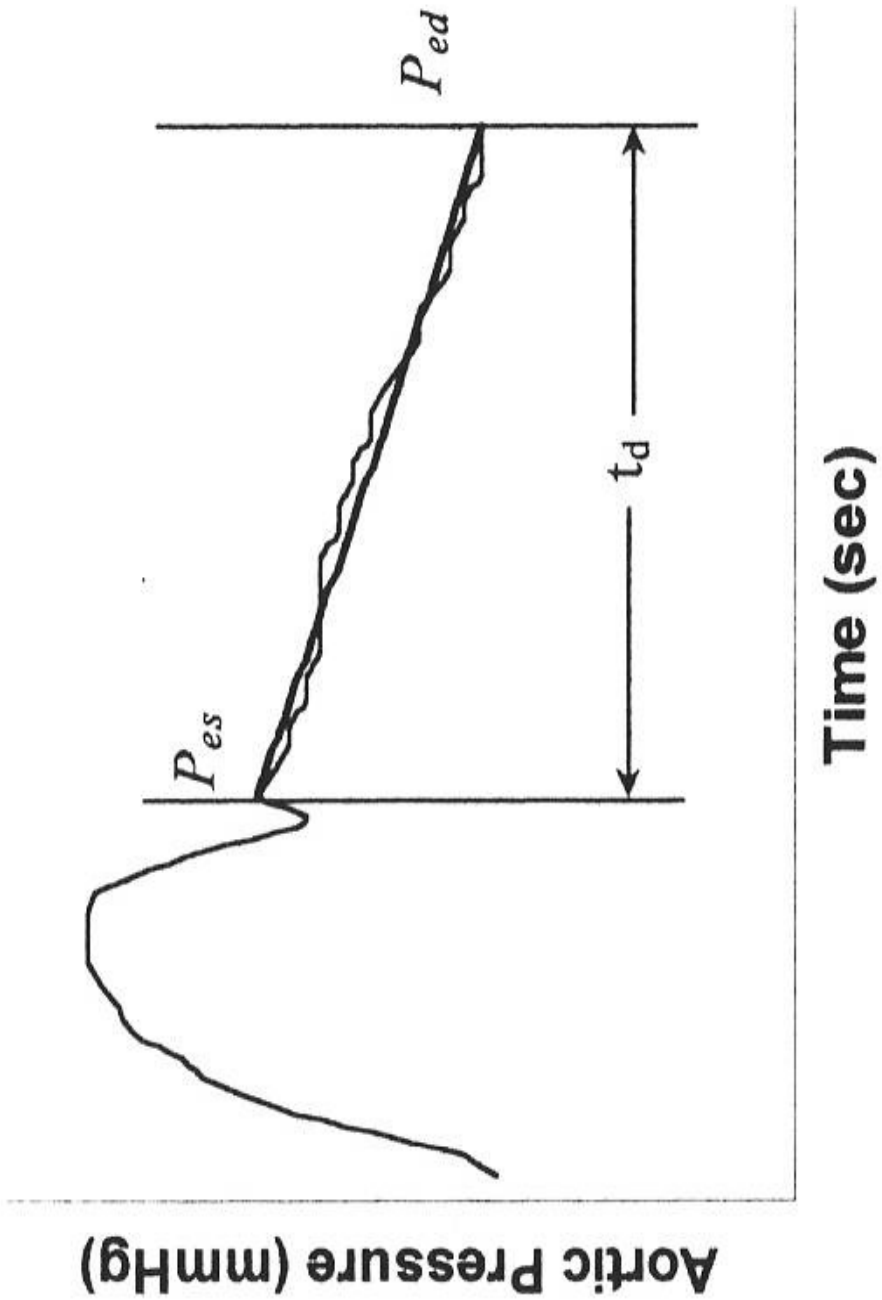

Figure 1.6 - Aortic pressure curve showing the parameters extracted to estimate the arterial compliance

1.4 Modeling the Cardiac System

Most fluid mechanic modeling assumes the fluid to be a Newtonian fluid – viscosity remains constant at constant temperature and pressure. Examples of Newtonian fluids are air, water and oil. Under most conditions, blood also behaves as a Newtonian fluid, thus the well established fluid mechanic principles can be applied to the circulatory system (Zamir 2000 p.13-15).

The cardiac system is essentially a pump (the heart) coupled to a highly branched pipe network (blood vessels). Modeling of the heart and the blood vessels and how these parts interact provides useful insight into the functioning of the body without excessive clinical studies.

Most current models are extended from the windkessel theory developed by Otto Frank (1899), which was based on hypothesis by Hales (1733) that the arteries must be elastic in order to accept the comparatively large stroke volume and they act as a reservoir to maintain the blood supply to the periphery during diastole. Figure 1.7 below illustrates the general windkessel theory.

In the windkessel models, the circulatory system is viewed from an electrical perspective. The blood pressure and flow are analogous to electrical voltage and current. Compliance of the arteries is represented as a capacitor. The total peripheral resistance (shown as its inverse, conductance, in Figure 1.7) equates to a resistor in parallel with the capacitor. These two components form the fundamental loads of the two element model proposed by Frank (1899).

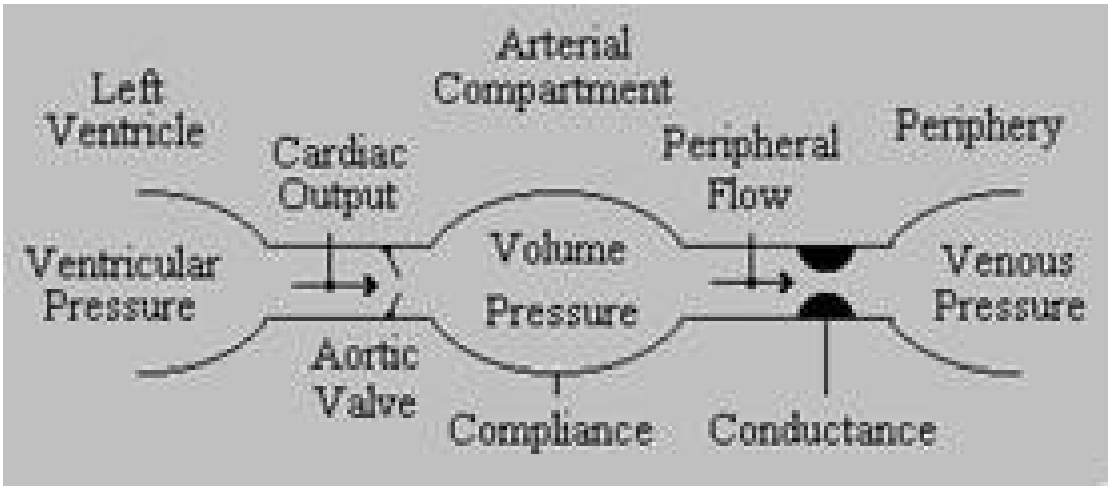

Figure 1.7 Illustration of the component s of windkessel model

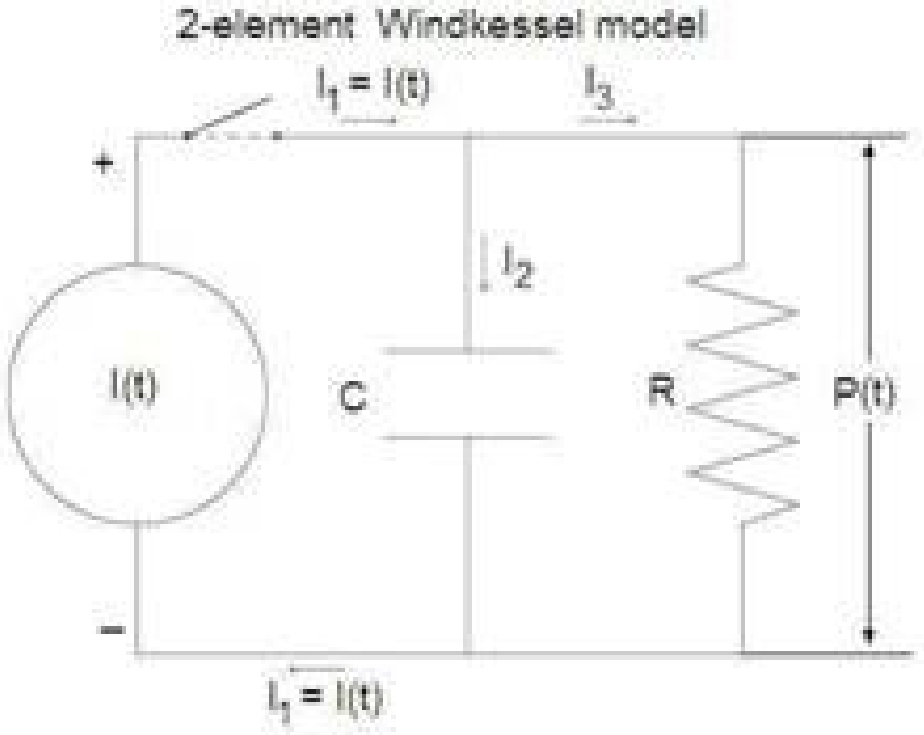

Figure 1.8 - Two element windkessel model with heart shown as current (flow) generator

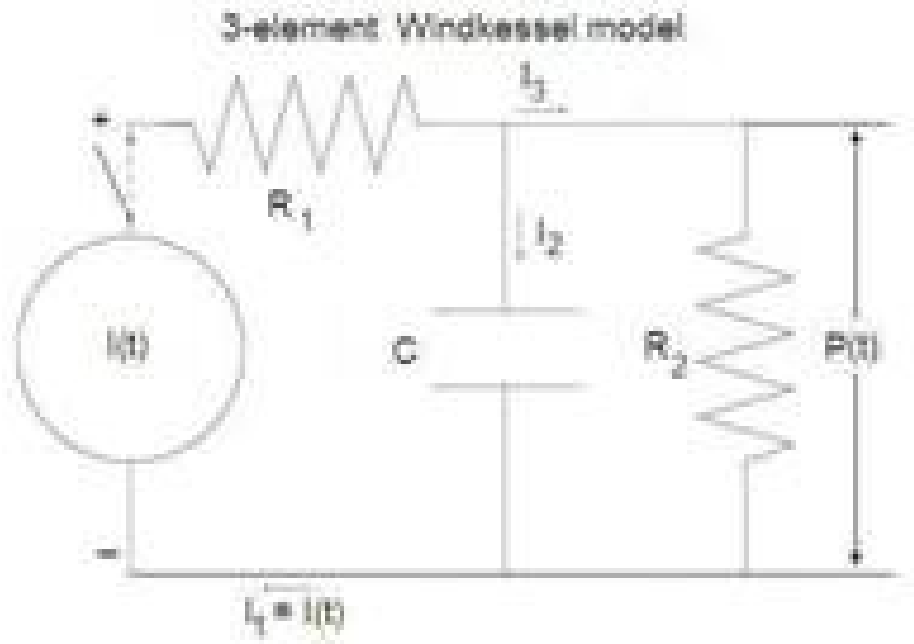

Figure 1.9 - Three element windkessel model

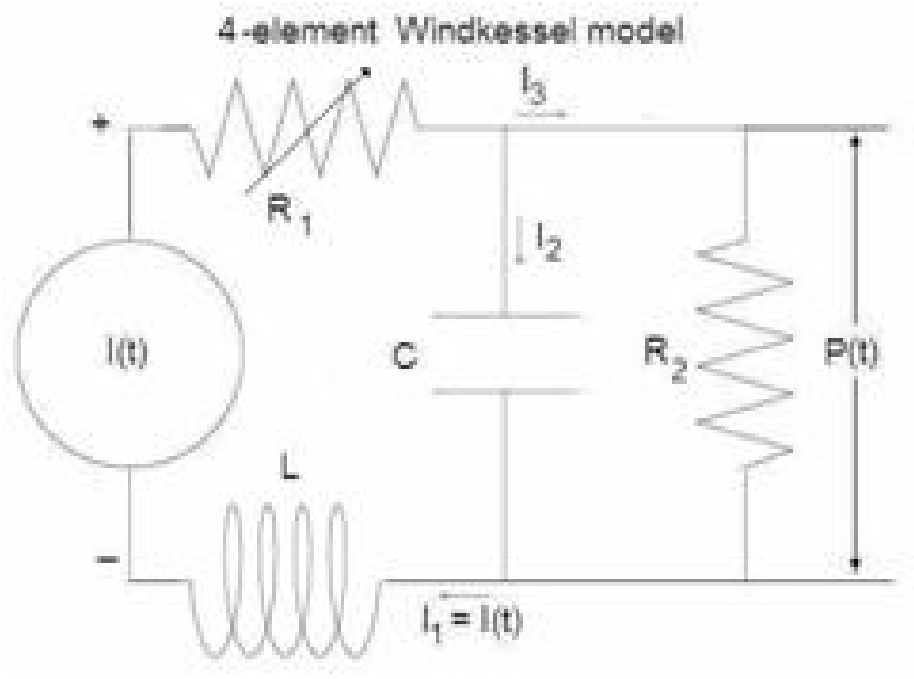

Figure 1.10 - Four element windkessel model

The three and four element models add a series resistor and an inductor successively. The series resistor represents the characteristic impedance of the proximal aorta, Z_0. The inductor equates to the inertance of the blood mass. These models are shown in Figures 1.9 and 1.10 on previous page. Westerhof et al (1969) introduced the three element model.

While the four element model provides a better fit to the data (Lambermont et al 1997), it is rarely used since the three element model provides good correlation with measured aortic pressure values with simpler first-order analysis (Geppel and Li, 1990; Quick et al., 1995).

The lumped windkessel model (Figure 1.11) provides a relatively efficient representation of the arterial system and its coupling with the left ventricle, treating the aortic pressure as the power source and taking into consideration the peripheral resistance and the compliance of the aortic segment. The compliance of the aortic segment far overshadows that of the remaining arteries, and as such there are no real gains from incorporating the compliance of other areas. The aortic valve resistance, $R_{v,}$ in drawing, can be considered a component of the characteristic impedance for simpler analysis. When this is done the pressure input to the proximal aorta is equivalent to the pressure supplied by the left ventricle.

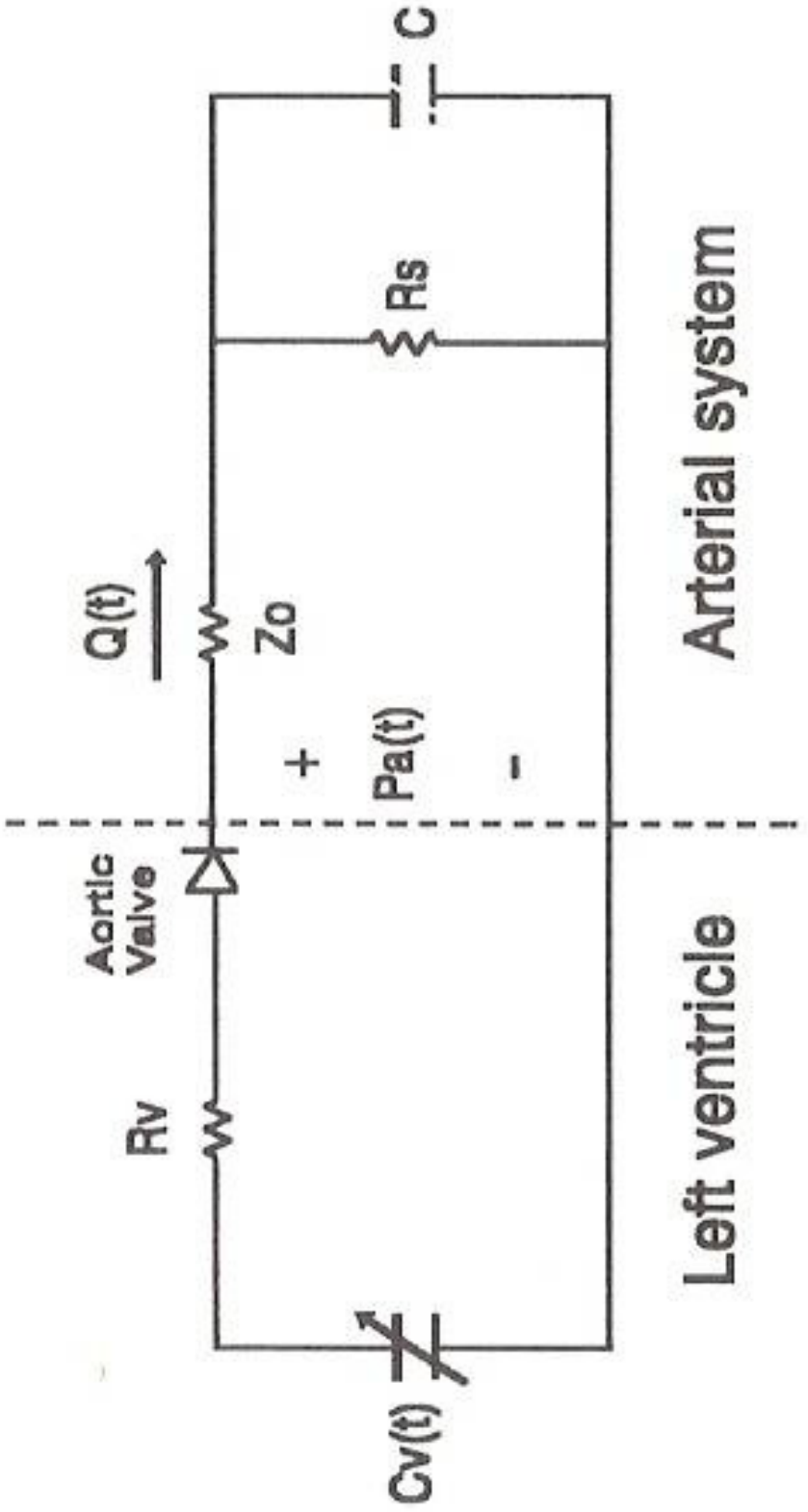

Figure 1.11 - Lumped-parameter model with 3 element Windkessel model of arterial system.

1.5 Pressure Waveform Analysis and Augmentation

Mahomed in 1872 demonstrated the importance of the pressure waveform as a diagnostic tool compared to simple systolic and diastolic pressure measurements. Since then, other investigators have derived important information from the pressure waveform (Westerhof et al., 1973; Van den Bos et al., 1976; O'Rourke and Gallagher, 1996).

The contribution of wave reflections to the central pressure waveform has garnered significant attention in recent years. Introduced by Murgo et al. in 1980, the augmentation index provides a simple approach to quantify this reflected pressure addition. In Murgo's method, the augmentation index is determined by examining the aortic pressure wave to determine the inflection pressure - that is the point at which the aortic pressure measured is being supplemented by the wave reflections. The pressure difference between the systolic pressure and the inflection pressure in then divided by the overall pulse pressure. The result is generally termed the augmentation index. In this thesis, the inflection pressure was considered to be the aortic pressure corresponding to the peak aortic flow, as opposed to being determined subjectively from the aortic pressure waveform.

The difference between the systolic pressure and the inflection pressure is simply termed augmentation. Fantin et al. proposed that augmentation was a better indicator of arterial stiffness than augmentation index based on a cross-sectional study of augmentation and augmentation index in the elderly population in the United Kingdom (Fantin et al., 2007).

Chapter 2. Aims and Significance

Heart disease, renal disease and stroke continue to be the leading causes of disability and mortality among adults in the United States of America. The pervasiveness of these disease processes is strongly related to the effects of many different risk factors; however, the number one culprit is that of hypertension. According to the Center for Disease Control's (CDC) National Center for Health Statistics, heart disease was responsible for the death of 700,142 American individuals in 2001 – this was the number one cause of death in the overall population. In 2005, there was only a minute decrease with 652,091 being the death toll for heart disease here in America, and it was still the number one cause of death.

As is the case with most disease processes, early detection affords early treatment thereby greatly improving the patient's chance of a positive outcome. Research has shown that pharmacological treatment of hypertension prevents or delays the development of heart failure and nephrosclerosis and reduces the incidence of stroke thereby prolonging life (Isles et al 1986).

There is no dividing line between normal and high blood pressure, arbitrary levels have been established to define persons who have an increased risk of developing a morbid cardiovascular event and/or will benefit from medical therapy (Harrison's et al 1998). Currently, clinical diagnosis of hypertension involves monitoring the blood pressure at the brachial artery, as measured with an arm cuff. The patient is then classified as hypertensive after diastolic readings above 90 mmHg and/or systolic reading in excess of 140 mmHg on three or more visits.

While the details of the role of hypertension in the clinical manifestations of atherosclerosis and other cardiovascular disease is still being researched, it is generally accepted that hypertension is a primary risk factor for the development cardiovascular disease. Atherosclerosis, a generalized disease of the arterial wall, is often referred to as hardening of the arteries and may progress or regress depending on several variables (Badimon et al 1993). Atherosclerosis is a dynamic process involving arterial wall remodeling and while it may go unnoticed for a lifetime, it can also present as acute vascular disease (Sierra et al 2008).

This thesis extends on previous works to identify possible cardiac health markers. Established methods of estimating aortic compliance are compared by evaluating each within the three element windkessel model and comparing the agreement of calculated pressure with measured values. The most robust compliance method is then used to derive the aortic volume change, which is then plotted against the aortic compliance in order to provide a direct comparison of compliance under normal, induced-hypertension and induced-vasodilation conditions.

Pulse pressure augmentation is currently viewed as a good candidate for indication of cardiovascular disease. The thesis proposes two new augmentation indices and compares them to three existing ones.

Chapter 3. Methods

3.1 Experiment (Data Acquisition)

Data was obtained from lab tests on mongrel dogs, conducted by Dr. Li and company. As described in their journal article (Li et al, 1990), the dogs were anesthetized and a catheter with a pressure reading tip was inserted, and a flow probe was positioned over the aorta. EKG leads were also attached to assist in timing the cardiac cycles. The signals were digitized and recorded through BIOPAC. Sodium nitroprusside and methoxamine were used to dilate and constrict the systemic vasculature, thereby simulating hypotension and hypertension respectively.

Experimental data were obtained from six mongrel dogs weighing between 20 – 24 kg. Each dog was anesthetized with intravenous Nembutal (pentobarbital sodium) (30 mg / kg) and ventilated through a tracheal tube with an external respirator. A left thoracotomy was performed at the fifth intercostals space isolating the ascending aorta, for placement of a cuff-type electromagnetic probe. A dual sensor Millar catheter-tip semiconductor pressure transducer was advanced in retrograde fashion through the femoral artery to the point at which the proximal sensor was positioned at exactly the same site as the flow probe or the simultaneous measurement of aortic and left ventricular pressure. The frequency response of the pressure transducer was uniform beyond 100 Hz and that of the flowmeter (Biotronex BL-610) was uniform within 5% to about 35 Hz. Lead II electrocardiogram, aortic pressure and flow signals were recorded simultaneously and later sampled at 10 ms intervals. This was done for all three test

conditions – control (steady-state), methoxamine induced vasoconstriction and sodium nitroprusside induced vasodilation.

Methoxamine is an alpha1-adrenoreceptor agonist that is commonly used to treat hypotension and shock (Klabunde, 2007). These receptors are found on the smooth muscle of blood vessels, and are normally activated by norepinephrine released from sympathetic nerves. When activated, the alpha1-adrenoreceptors induce contraction of the smooth muscles, thereby constricting the blood vessels. Since the methoxamine acts directly on the systemic blood vessels, without sympathetic nervous stimulation, the heart rate and contractility are not directly affected (the heart has beta-adrenergic receptors). While both arteries and veins are affected by the alpha-agonist, the greater muscle content of the arteries results in a more pronounced effect within the arterial system.

Sodium nitroprusside acts on the systemic vessels via spontaneous release of nitric oxide. Nitric oxide, normally produced by the endothelial cells of blood vessels, ultimately brings about dilation of the blood vessels, by relaxing the smooth muscles. The physiological details of this signaling action were described by Furchgott, Ignarro and Murad; this work earned them the 1998 Nobel Prize in Physiology or Medicine. Sodium nitroprusside is used in hypertensive emergencies since it acts rapidly (Klabunde 2007).

3.2 Windkessel model

The three element windkessel model with pressure-dependent compliance has been shown to be an accurate model of the arterial system (Li, 2000).

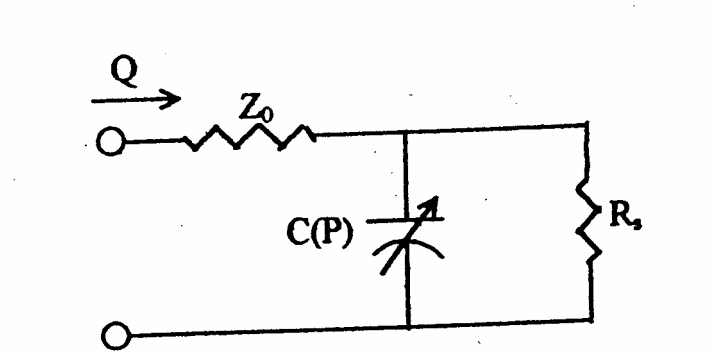

Figure 3.1 - Three element windkessel model - electrical analog

The electrical circuit analogy yields the following equations:

(3.1) $$Q_{ao}(t) = Q_{R_S}(t) + Q_c(t)$$

(3.2) $$Q_C(t) = C * \frac{dP(t)}{dt}$$

(3.3) $$Q_{R_S}(t) = \frac{P_S(t)}{R_S}$$

$Q_c(t)$ is the flow through the compliance section
$Q_{R_S}(t)$ is the flow through the resistive section
$Q_{ao}(t)$ is the flow through the ascending aorta (corresponds to measured flow)

From the above three equations we can deduce that,

(3.4) $$\frac{dP(t)}{dt} = \frac{1}{C}\left[Q_{ao}(t) - \frac{P(t)}{R_S} \right]$$

By discrete approximation of Equation 3.4, we can compute the aortic pressure from aortic flow and initial pressure (diastolic pressure). This is shown in equation 3.5.

(3.5) $$P_{i+1} = P_i + \frac{dt}{C}\left(Q_i - \frac{P_i}{R_s} \right)$$

Peripheral resistance was determined as the mean aortic pressure divided by the mean aortic flow. The characteristic impedance of the system was determined as the ratio of pressure to flow during the ejection phase – the first five sample points of each data set were used to this effect. The compliance was found by the three methods outlined in Chapter 1.

The model was implemented with MATLAB 5.3

3.3 Aortic Volume

Since an aortic volume data set was not available, the aortic volume at the end of systole estimated to be the stroke volume derived by integrating the aortic flow over one cardiac cycle.

The aortic volume change was determined directly from the compliance

(3.6) $$dV = CdP$$

Therefore discrete approximation yields

(3.7) $$dV = C(P_{i+1} - P_i)$$

3.4 Wave reflections and Resultant Pressure Pulse Augmentation

The amplification of the pressure pulse by virtue of wave reflections was denoted in the nineteenth century by Spengler (1843) and Von Kries (1892). Since then, several researchers have studied the location of reflections and the waveform of the reflected pressure pulse (Cox and Pace, 1975); van den Bos et al., 1976; Li, 1978; Murgo et al., 1980, 1981; Li et al., 1984b.

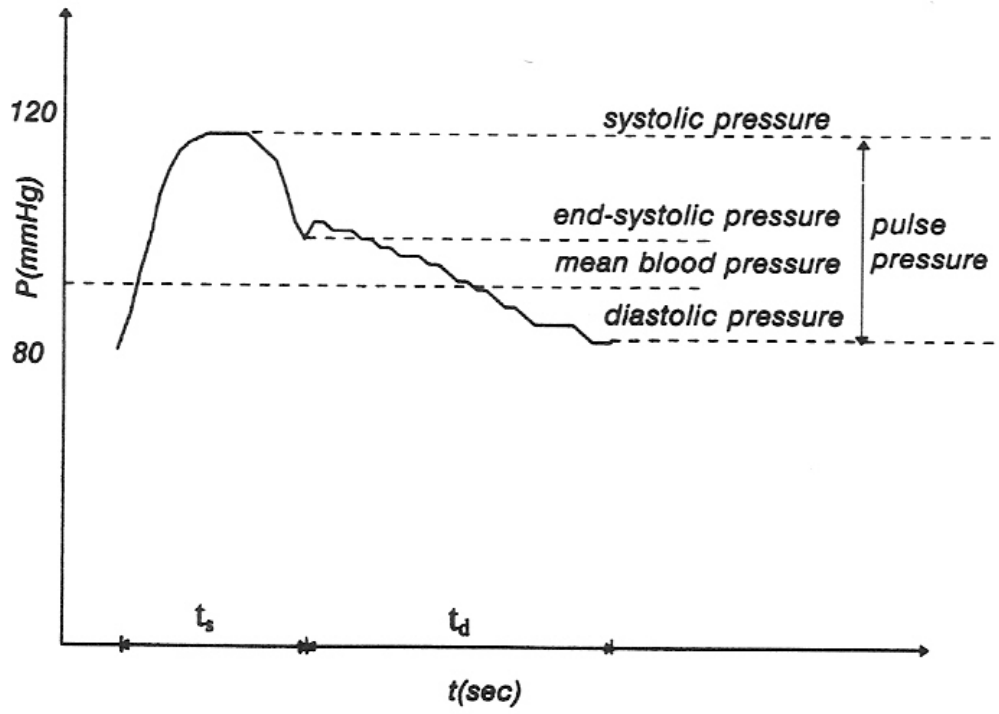

Figure 3.2 - Representative aortic pressure curve

The reflected pressure wave contributes significantly to the overall aortic pressure especially in late systole. This contribution is termed augmentation. The aortic pressure at peak flow is the pressure at the inflection point of curve, P_{inf}.

(3.8) $$Aug = P_{\max} - P_{\inf}$$

The augmentation index labeled AIA was then determined by dividing the augmentation by the pulse pressure.

(3.9) $$AIA = \frac{Aug}{(P_s - P_{ed})}$$

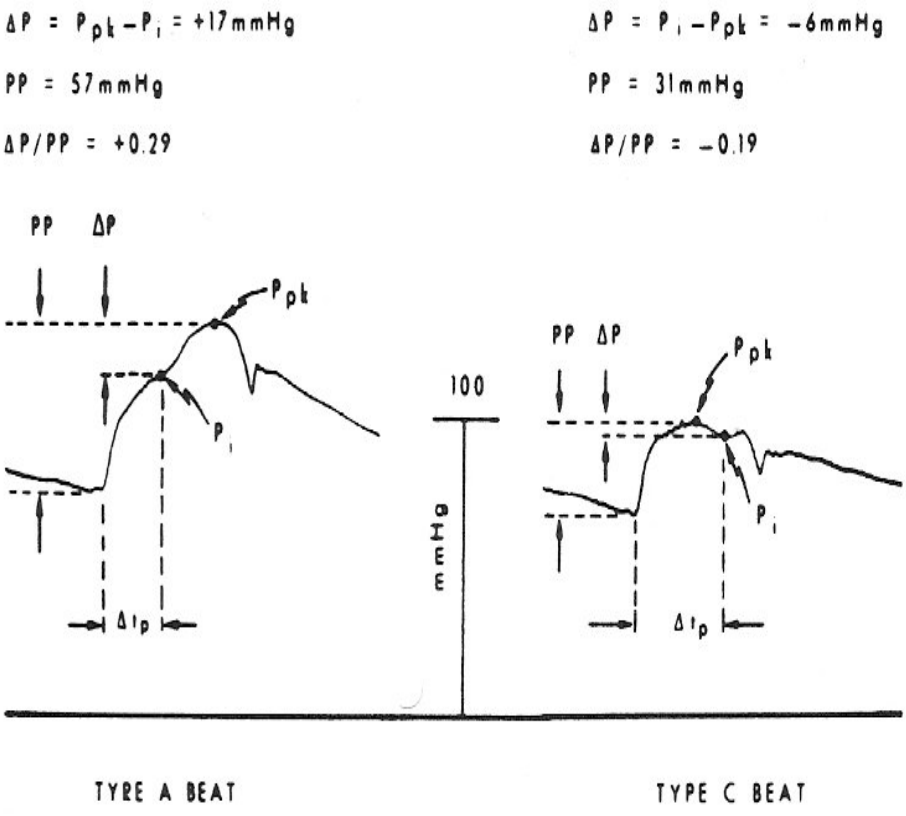

Figure 3.3 - Augmentation and Augmentation Index A for different beat types

The other augmentation index, AIB was determined from the resolved forward and reverse pressure waves. Equations 3.8 and 3.9 give the forward or antegrade and reflected or retrograde pressure waves respectively.

(3.10) $$P_f = \frac{\left(P + Q \times Z_0\right)}{2}$$

(3.11) $$P_r = \frac{\left(P - Q \times Z_0\right)}{2}$$

(3.12) $$AIB = \frac{P_r \max}{P_f \max}$$

(3.13) $$PP_r = P_r \max - P_r \min$$

(3.14) $PP_f = P_f \max - P_f \min$

(3.15) $AIC = PP_r$

(3.16) $AID = {PP_r}/{PP_f}$

Chapter 4. Results

4.1 Compliance Estimations Comparison

The comparisons of compliance estimation methods are based on ability to accurately derive aortic pressure from flow. The graphs show the measured pressure and flow waveforms along with the derived pressure. The root-mean-square-error is shown on each graph for the various compliance models used.

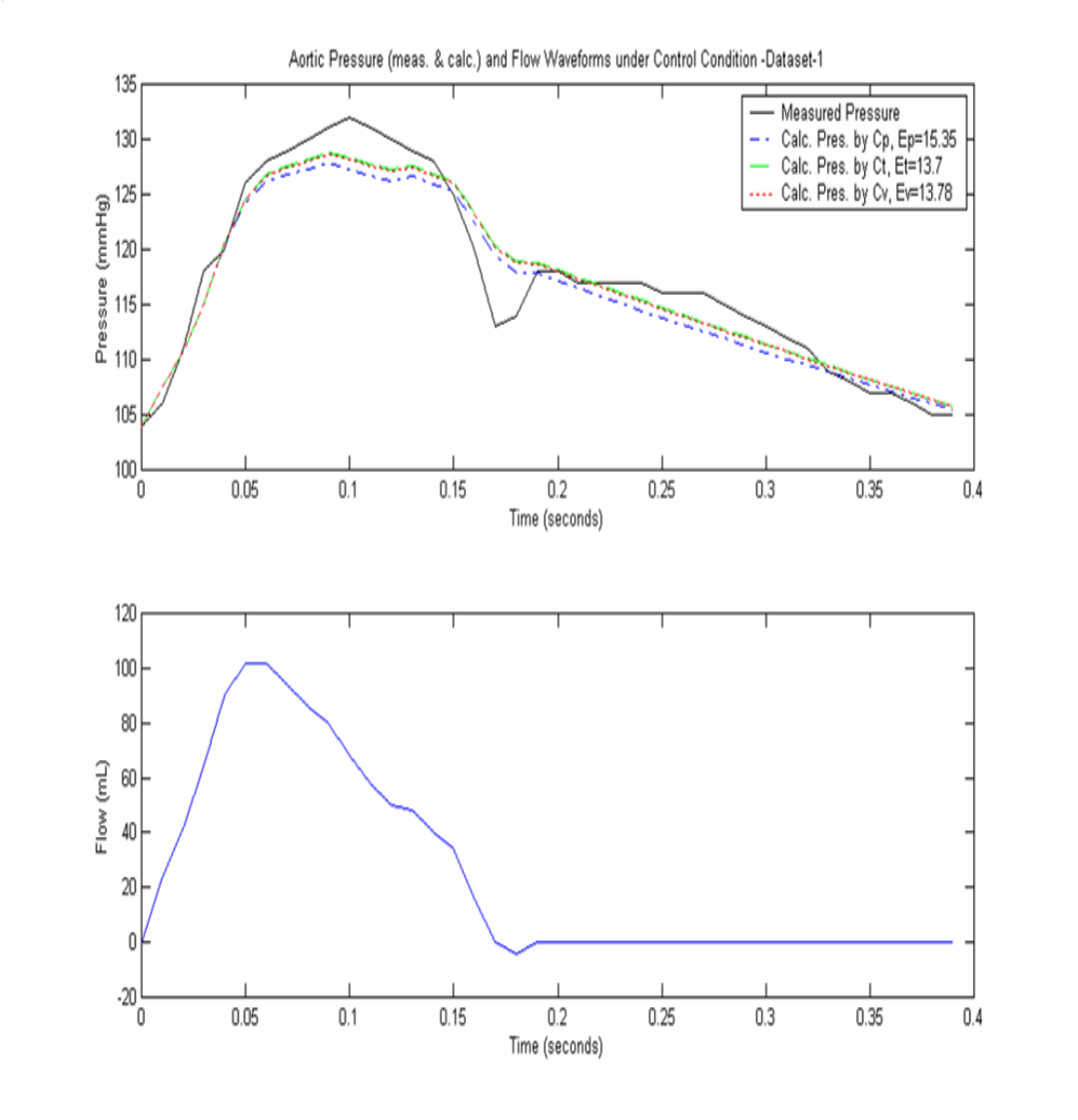

Figure 4.1 - Aortic flow (below) and calculated vs. measured pressure for control condition. Dataset 1.

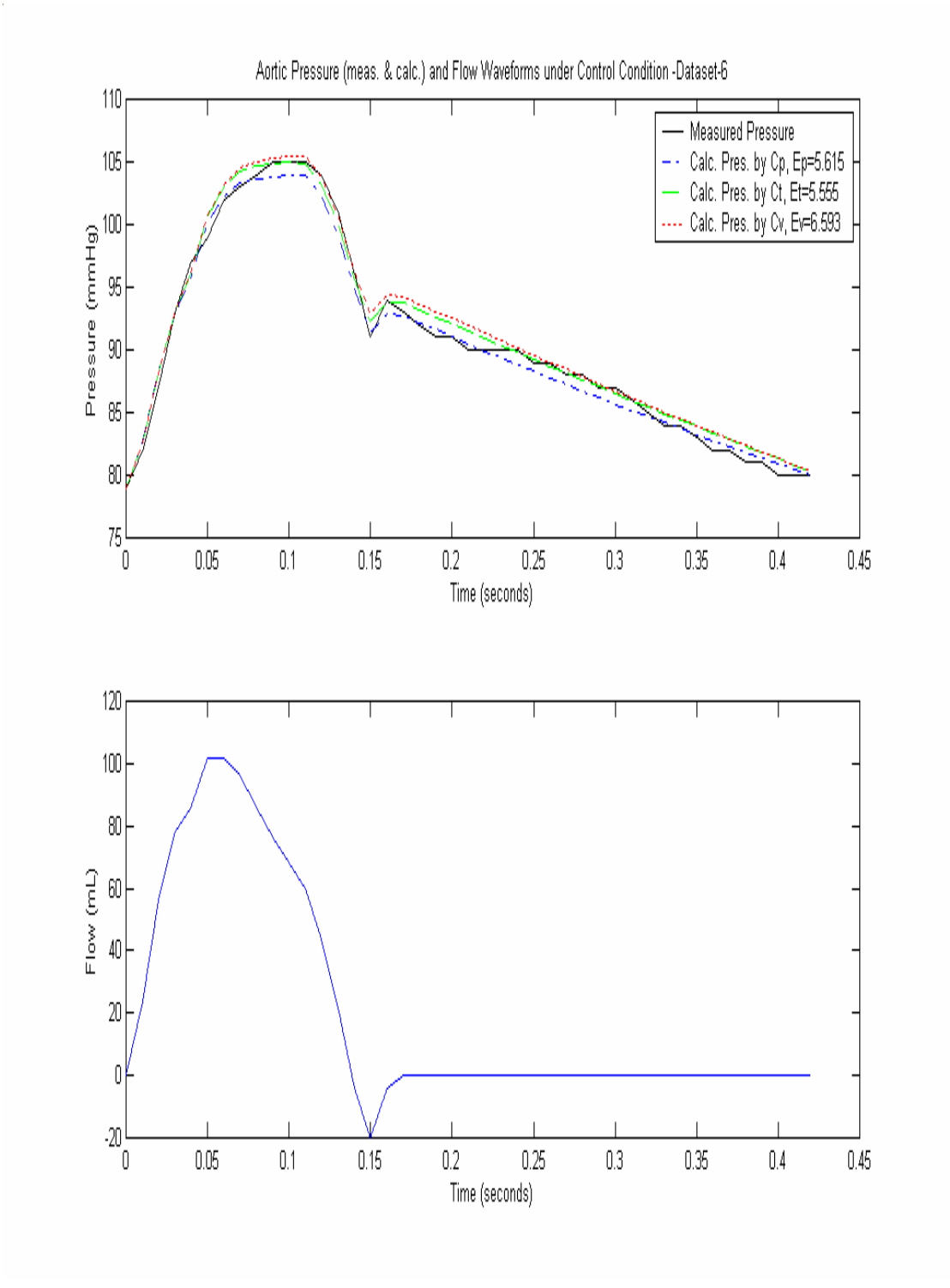

Figure 4.2 - Aortic flow (below) and calculated vs. measured pressure for control condition. Dataset 6.

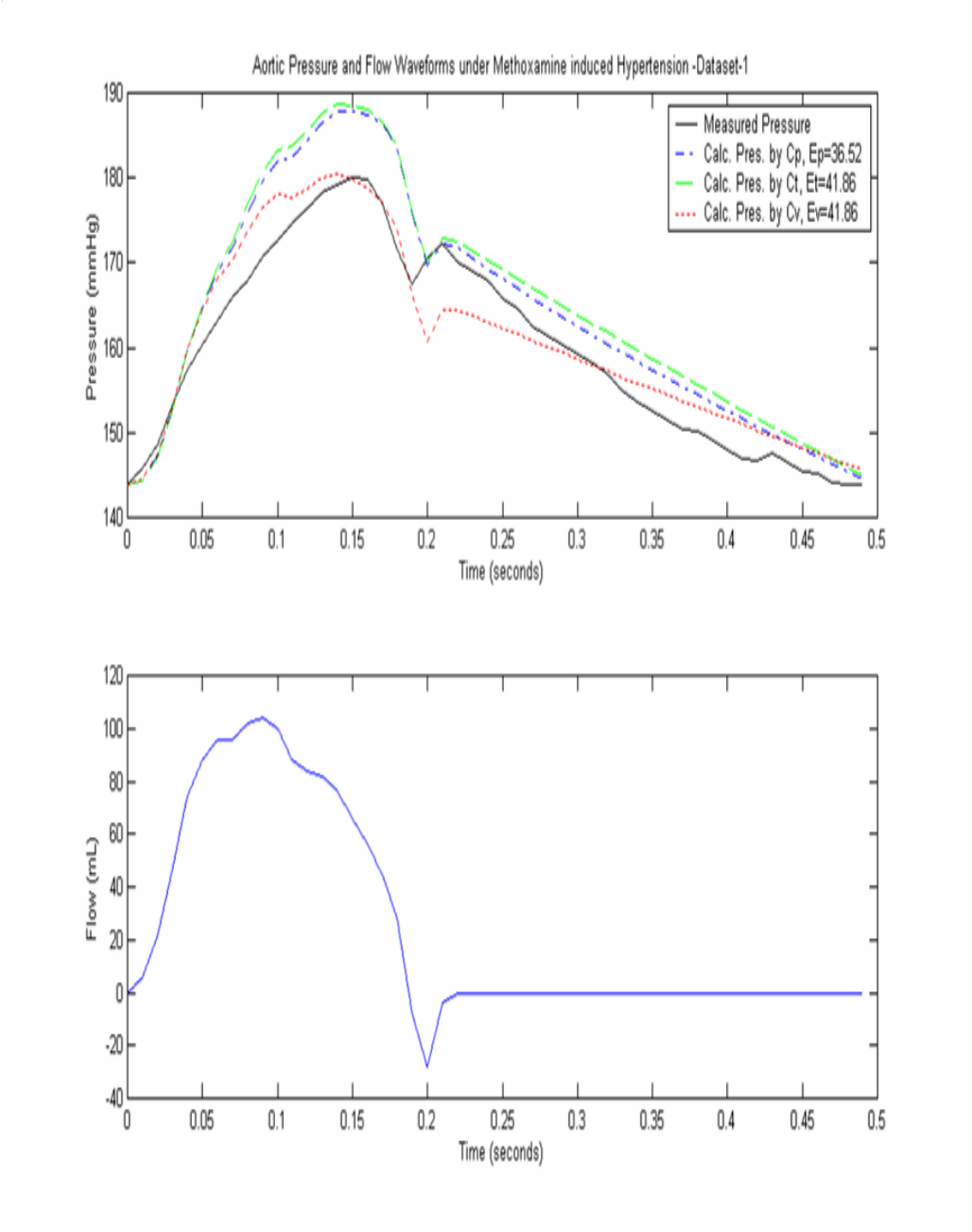

Figure 4.3 - Aortic flow (below) and calculated vs. measured pressure for MTX condition. Dataset 1

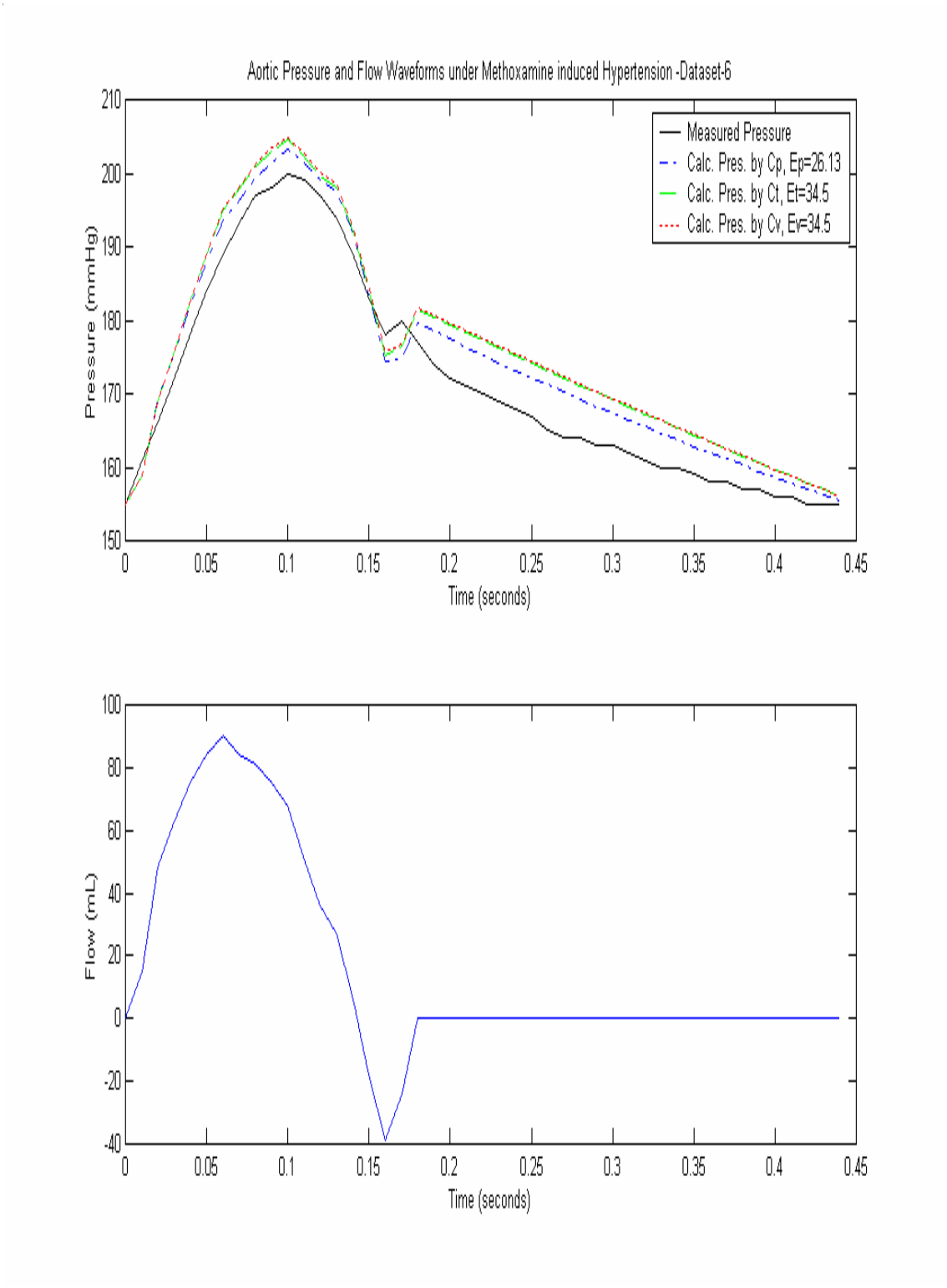

Figure 4.4 - Aortic flow (below) and calculated vs. measured pressure for MTX condition. Dataset 6

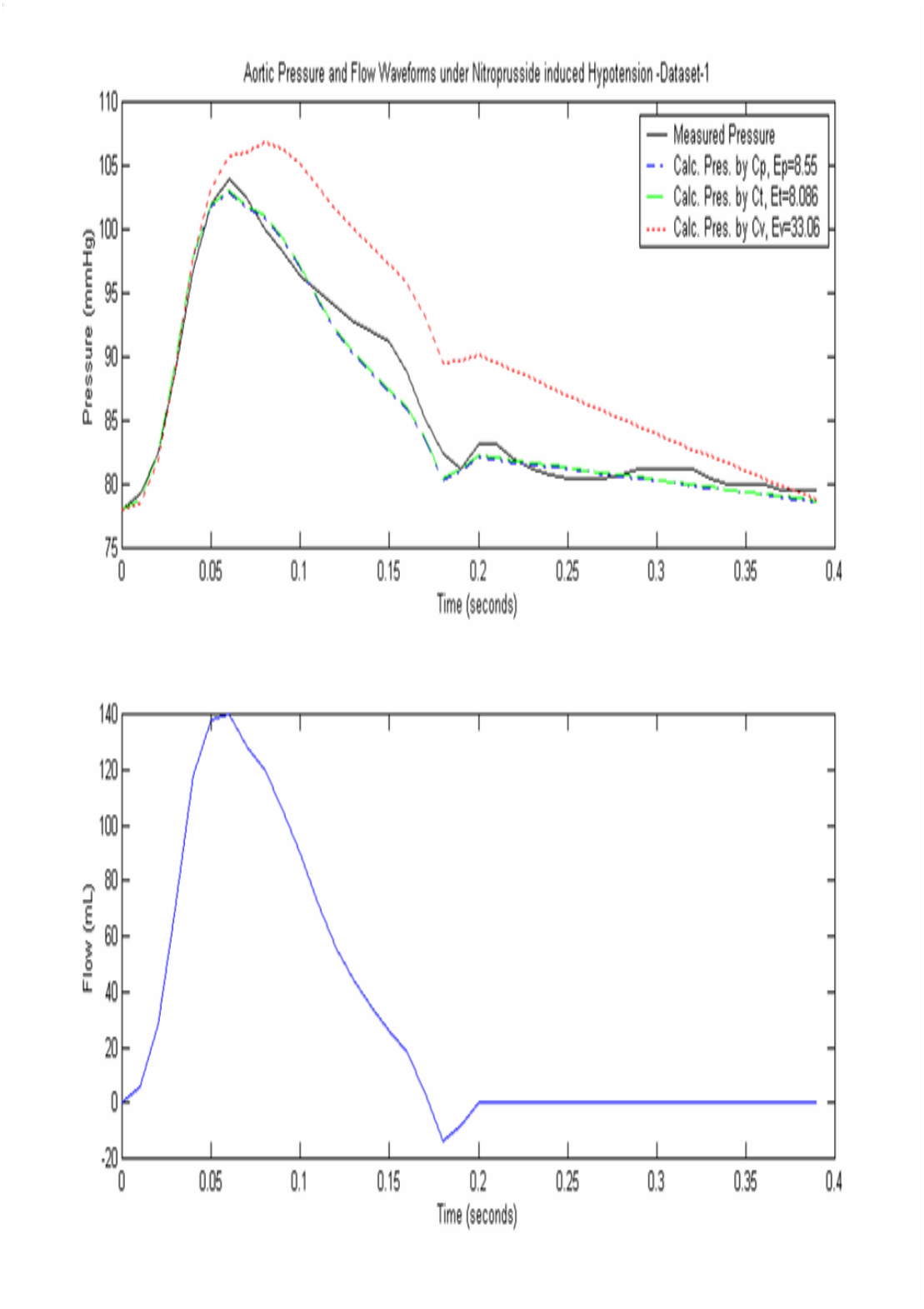

Figure 4.5 - Aortic flow (below) and calculated vs. measured pressure for NTP condition. Dataset 1

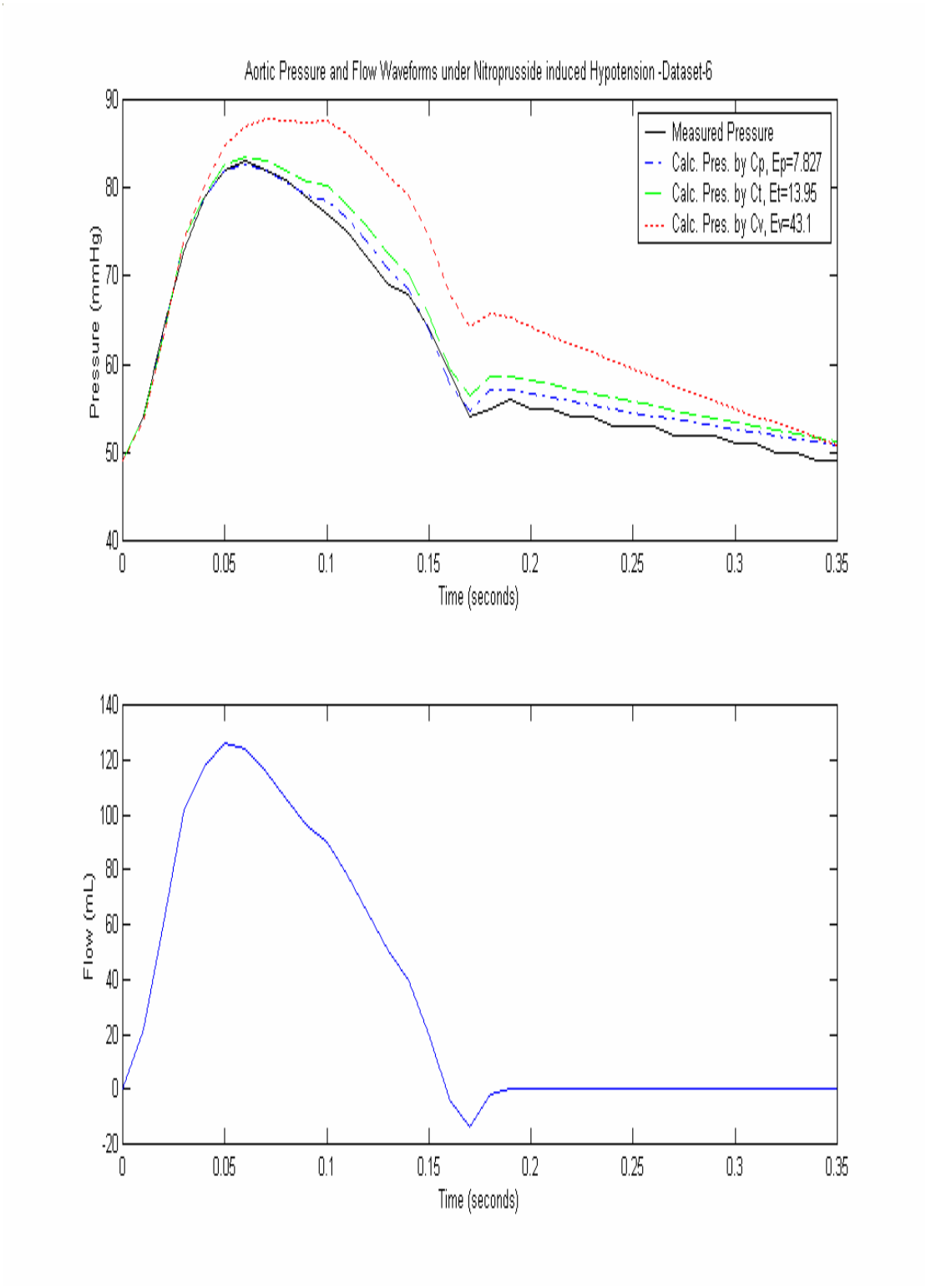

Figure 4.6 - Aortic flow (below) and calculated vs. measured pressure for NTP condition. Dataset 6

A general overview of the previous graphs reiterates the efficacy of the three element windkessel model. The graphs also indicate the increase in mean arterial pressure and increased pulse pressure with induced hypertension. The mean arterial pressure decreased in vasodilated state and pulse pressure also decreased slightly

The error values for the three different compliance methods provide the basis of comparison. From this perspective, the compliance estimated by the stroke volume method, C_v, was the least efficient, consistently yielding the largest error.

The pressure dependent compliance model yielded the most consistently accurate model for the aortic pressure. It provided the closest matching curve in Figures 4.3, 4.4 and 4.6, and in the other three curves it was a close second to the time constant method compliance, C_t.

These results illustrate why the pressure dependent model was used in the subsequent analysis of aortic volume change.

4.2 Aortic pressure-volume relation

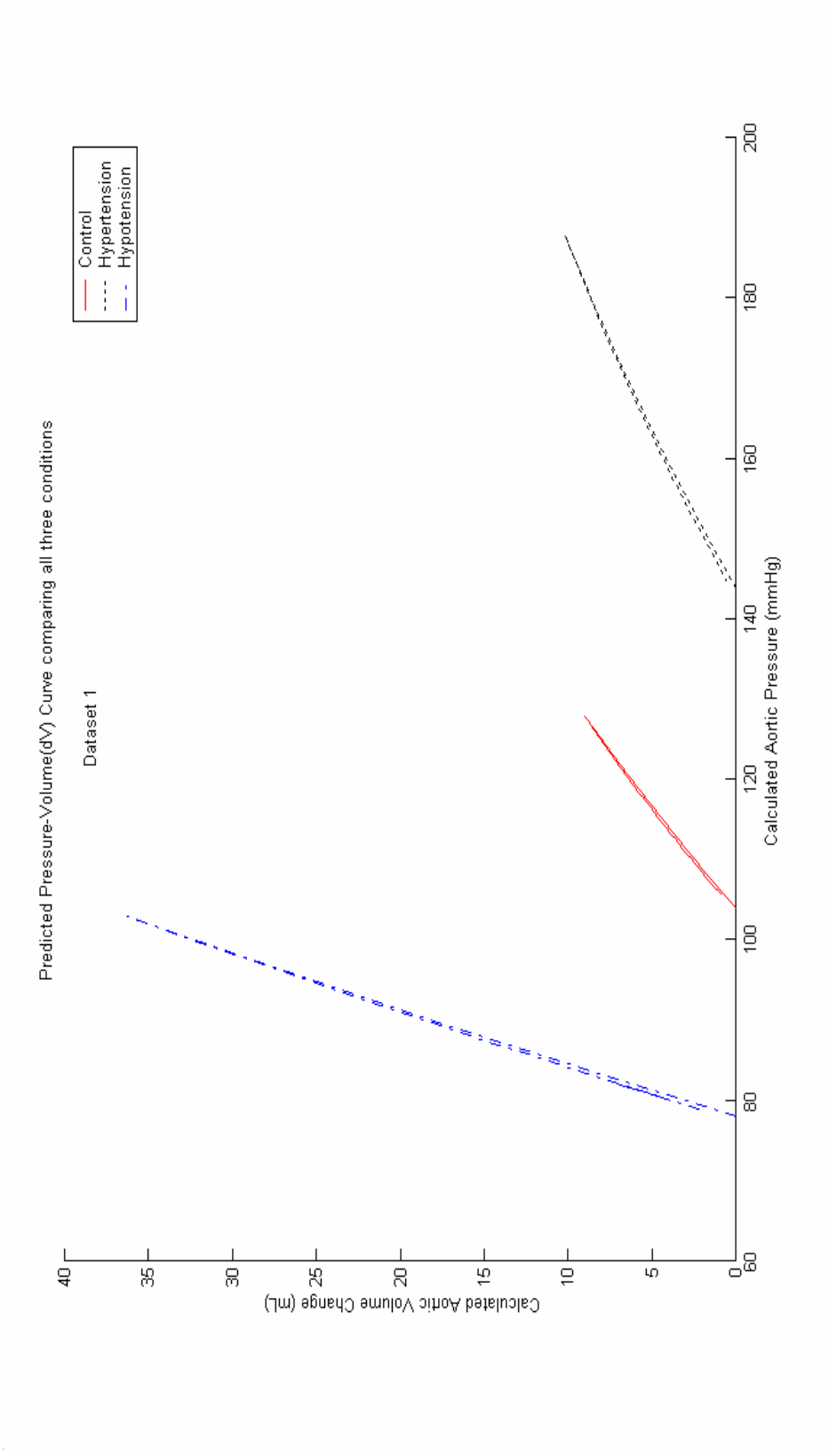

Figure 4.7 – Calculated aortic volume change vs. aortic pressure. Dataset 1

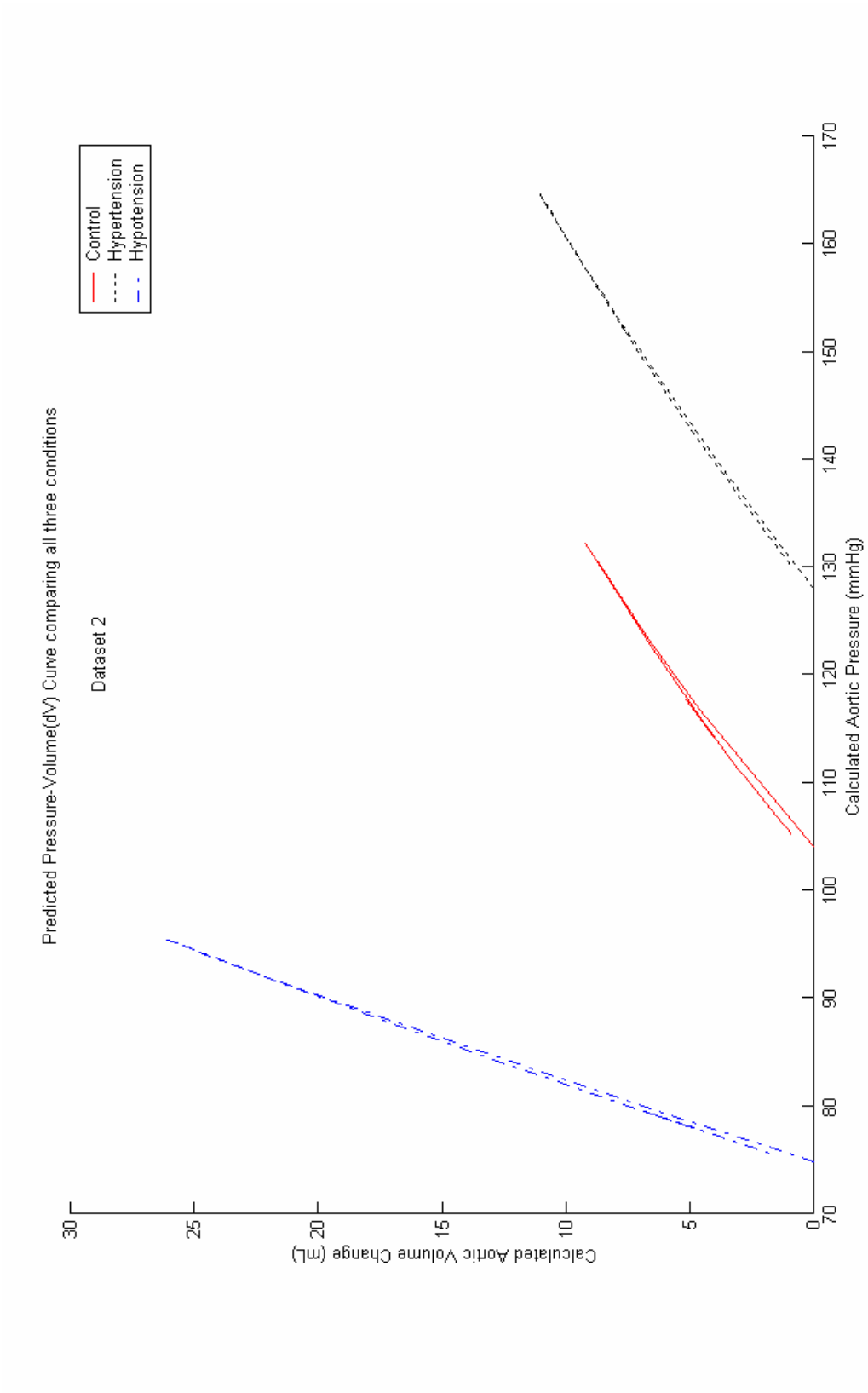

Figure 4.8 - Calculated aortic volume change vs. aortic pressure. Dataset 2

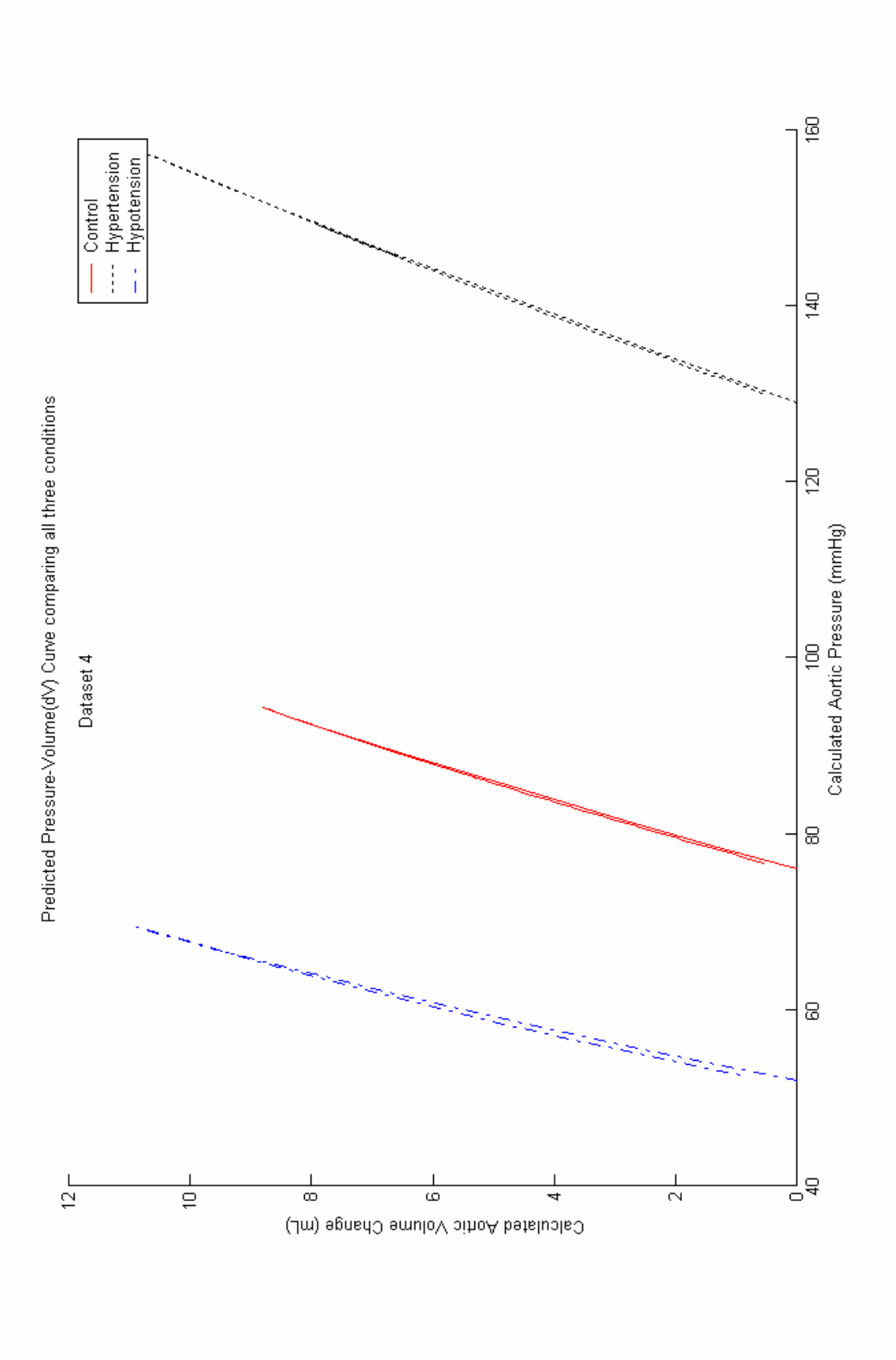

Figure 4.9 - Calculated aortic volume change vs. aortic pressure. dataset 4

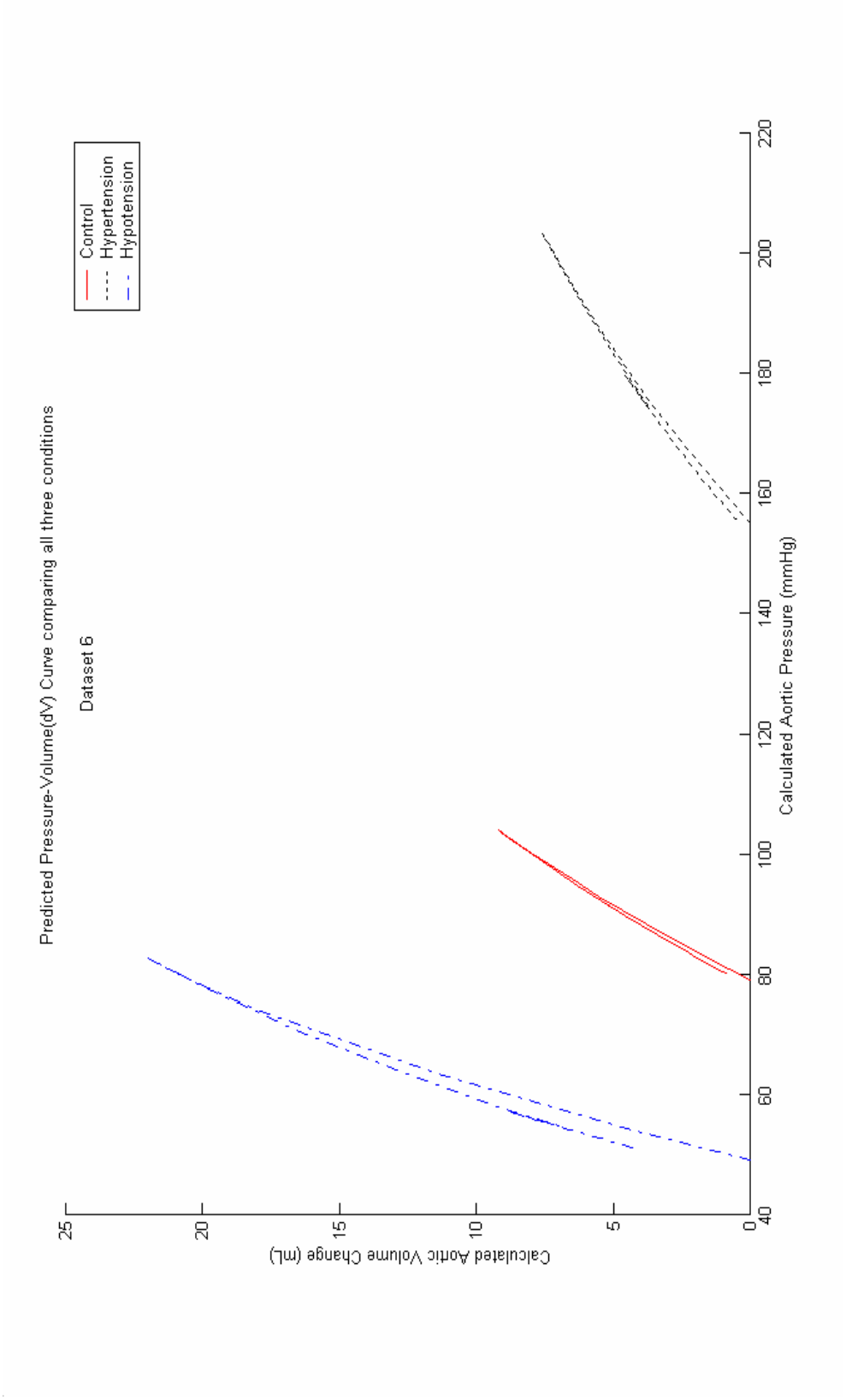

Figure 4.10 - Calculated aortic volume change vs. aortic pressure. dataset 6

From the results of the Aortic volume change–aortic pressure curves, we see that the hysteresis of the volume response, while evident, was negligible. For the fixed compliance methods these curves would be similar, without any curvature.

A decrease in compliance is seen as a decrease in the average slope of the volume-pressure curve and a steep average slope shows a high compliance.

In all but Dataset 4, the aortic volume change during nitroprusside induced vasodilation was at least double that of the other conditions. The slope of the vasodilated condition was consistently the steepest, whereas the slope of the methoxamine induced hypertension was the lowest in all cases.

In general the results agree with the accepted conclusion that in the hypertensive state, compliance is reduced and in the hypotensive state compliance in increased.

4.3 Augmentation Indices

Recall relevant equations from Chapter 1:

Augmentation, $Aug = P_{\max} - P_{\inf}$

Augmentation Index A $AIA = \dfrac{Aug}{(P_s - P_{ed})}$

Antegrade pressure wave $P_f = \dfrac{\left(P + Q \times Z_0\right)}{2}$

Retrograde pressure wave $P_r = \dfrac{\left(P - Q \times Z_0\right)}{2}$

Augmentation Index B $AIB = \dfrac{P_r \max}{P_f \max}$

Pulse pressure of retrograde wave $PP_r = P_r \max - P_r \min$

Pulse pressure of antegrade wave $PP_f = P_f \max - P_f \min$

Augmentation Index C $AIC = PP_r$

Augmentation Index D $AID = PP_r \big/ PP_f$

	Augmentation			Augmentation Index A			Augmentation Index B			Aug Index C = PPr			Aug Index D = PPr/PPf		
Dataset	Control	MTX	NTP	Control	MTX	NTP	Control	MTX	NTP	Control	MTX	NTP	Control	MTX	NTP
Set1	6.000	9.260	0.000	0.222	0.256	0.000	0.834	0.900	0.680	9.759	17.822	4.969	0.469	0.680	0.200
Set2	3.000	15.000	2.400	0.120	0.469	0.091	0.802	0.901	0.714	7.980	15.364	6.276	0.362	0.643	0.271
Set4	3.000	9.000	0.000	0.158	0.346	0.000	0.814	0.927	0.671	5.776	12.809	2.750	0.384	0.693	0.167
Set6	6.000	11.000	1.000	0.240	0.244	0.029	0.815	0.856	0.526	9.890	19.485	6.250	0.490	0.581	0.192
Mean	4.500	11.065	0.850	0.185	0.329	0.030	0.816	0.896	0.648	8.351	16.370	5.061	0.426	0.649	0.208
Std dev	1.732	2.770	1.136	0.056	0.104	0.043	0.013	0.029	0.083	1.925	2.916	1.657	0.063	0.050	0.045
P-one tail (t-test)		5.06E-03	8.42E-03		2.95E-02	2.28E-03		3.87E-03	1.41E-02		2.95E-03	2.06E-02		7.35E-04	1.18E-03
P (t-test) mean	6.74E-03			1.59E-02			8.97E-03			1.18E-02			9.59E-04		
P-value (ANOVA)	1.60E-04			8.81E-04			4.57E-07			1.54E-04			3.48E-06		

Table 4-1 - Augmentation Indices of Datasets with corresponding means, standard deviations and P-values for ANOVA and Student t-test (compared to Control for corresponding condition).

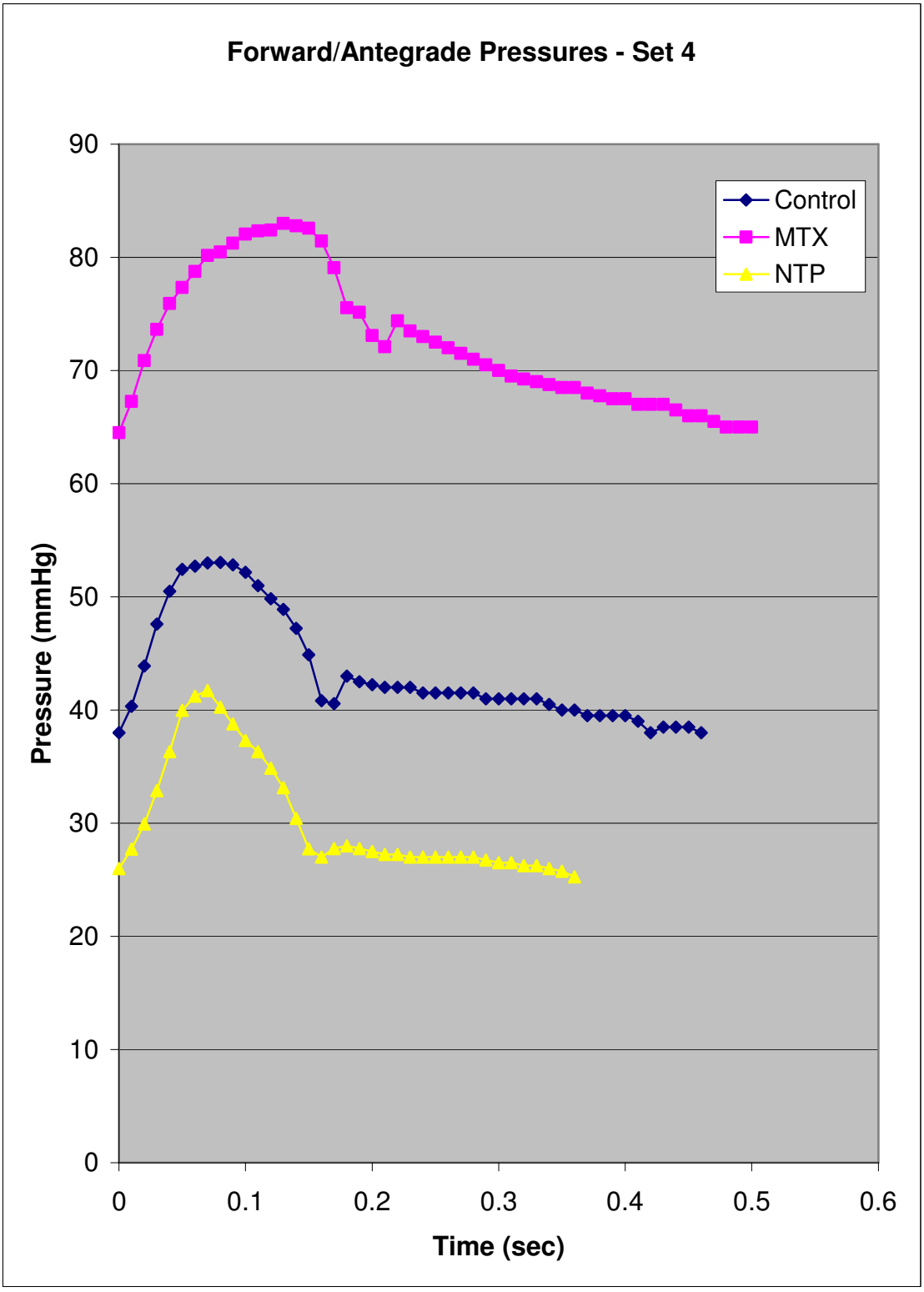

Figure 4.11 - Forward Pressure Waves

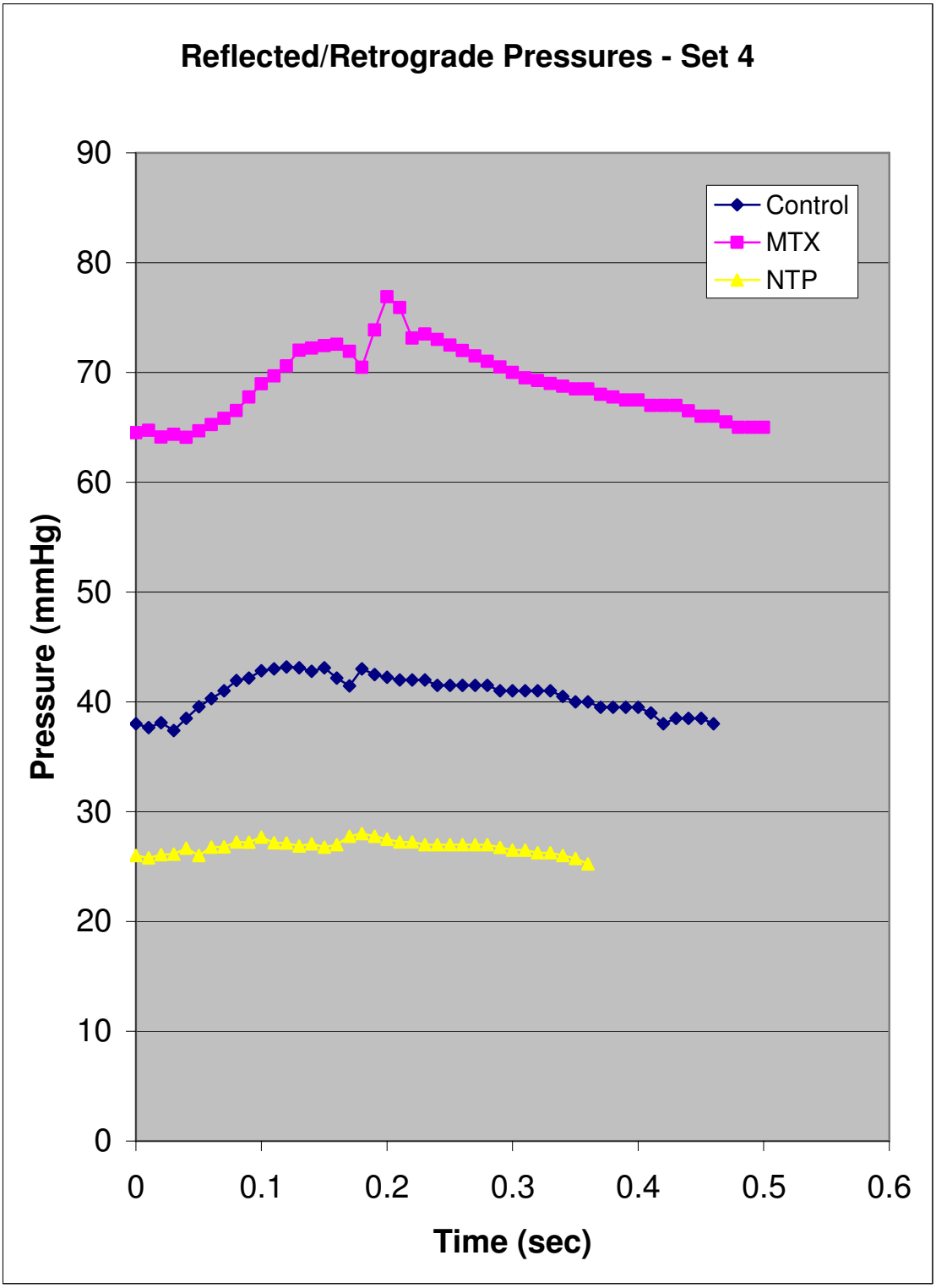

Figure 4.12 - Reflected Pressure Waves

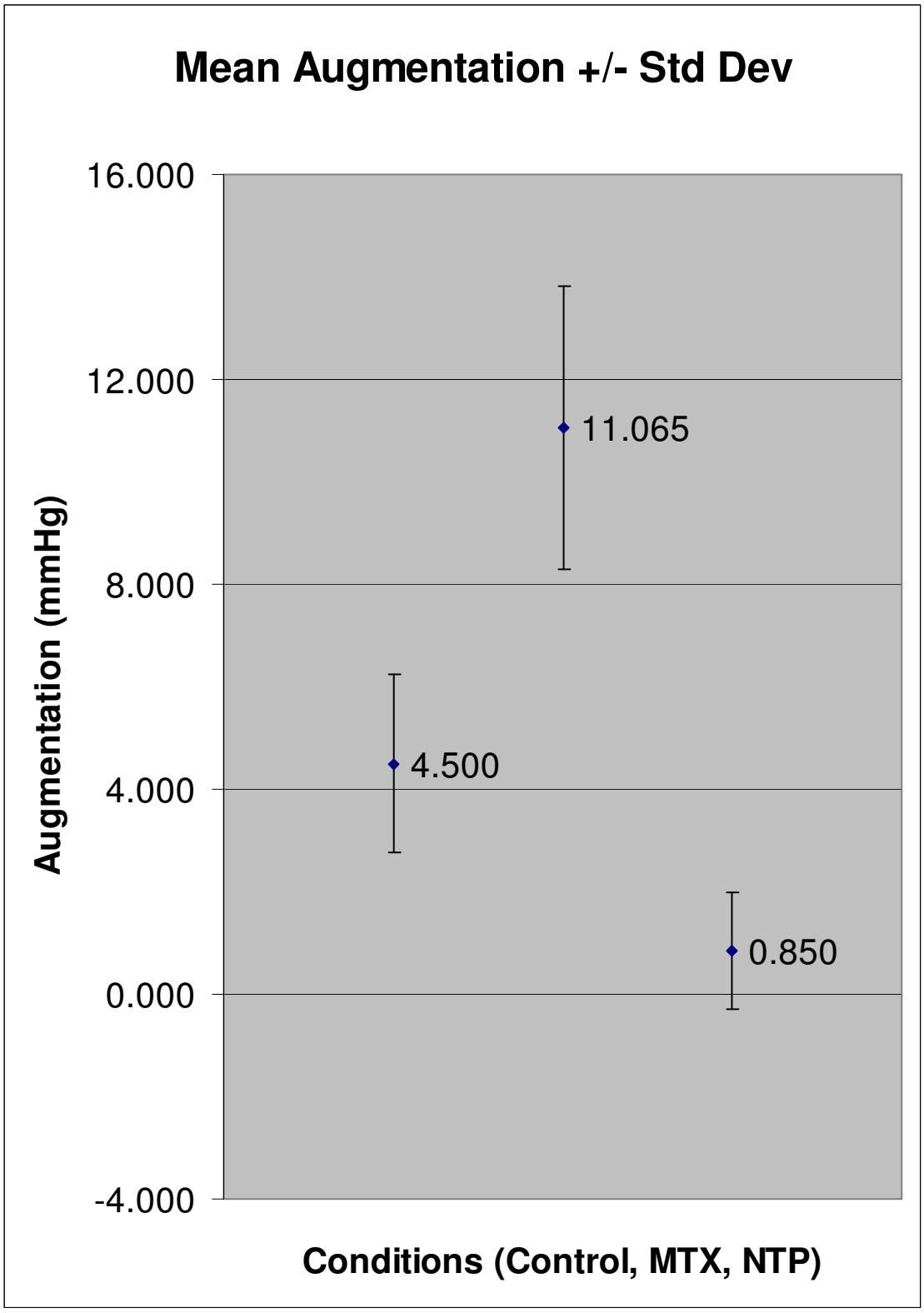

Figure 4.13 - Average Augmentation for four datasets

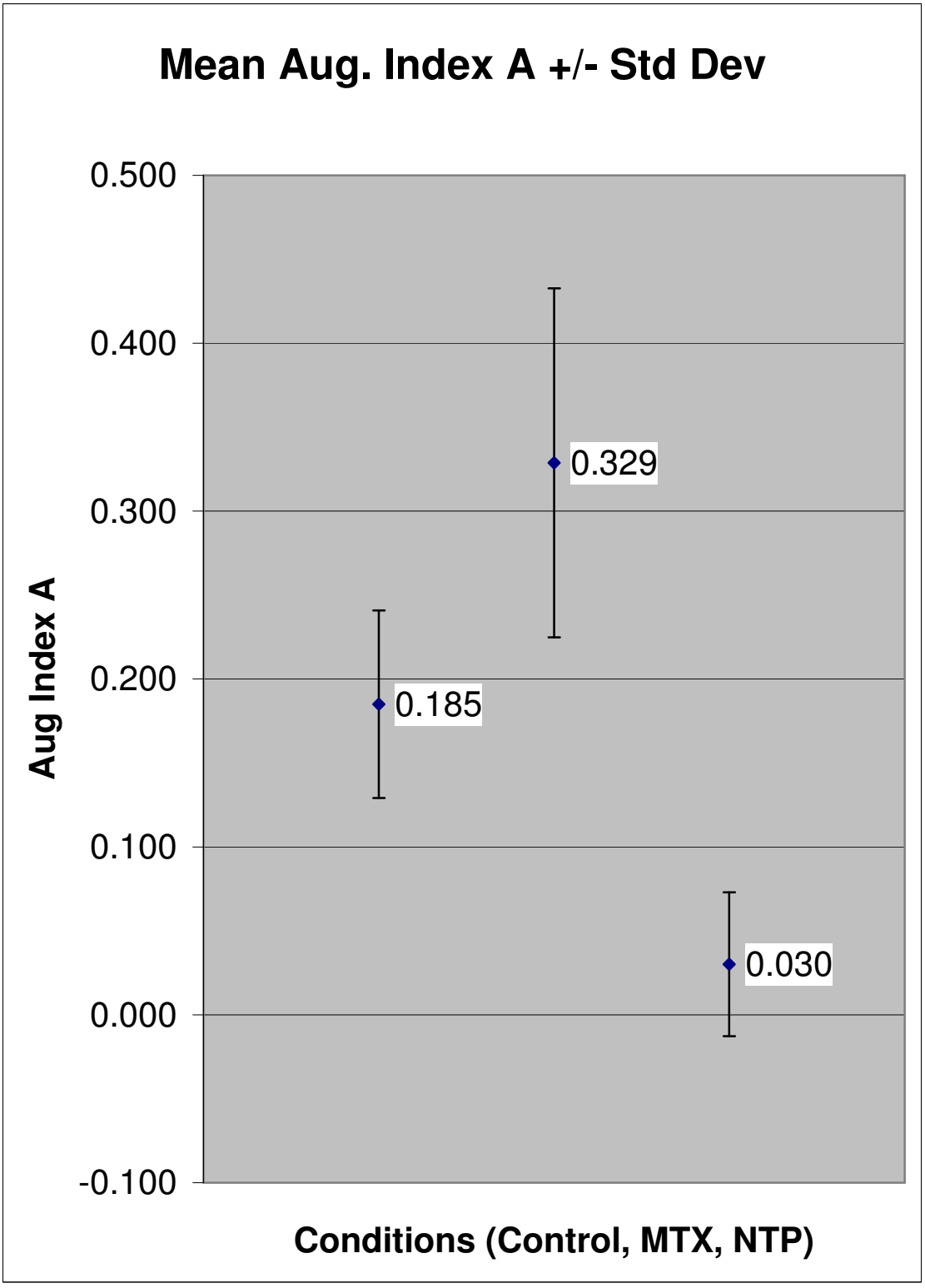

Figure 4.14 - Average Augmentation Index A (AIA) - most popular index

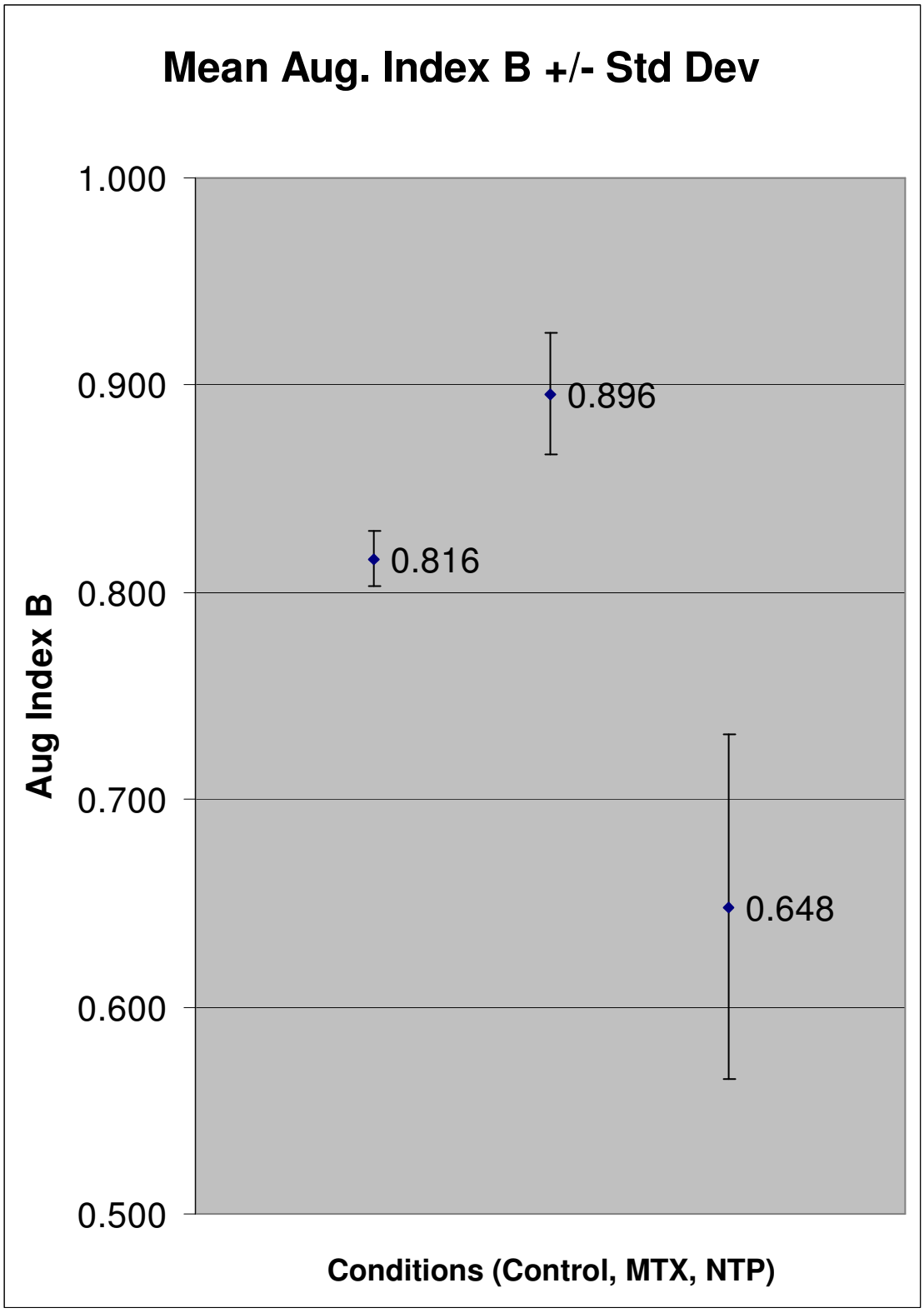

Figure 4.15 - Average Augmentation Index derived by method B (AIB)

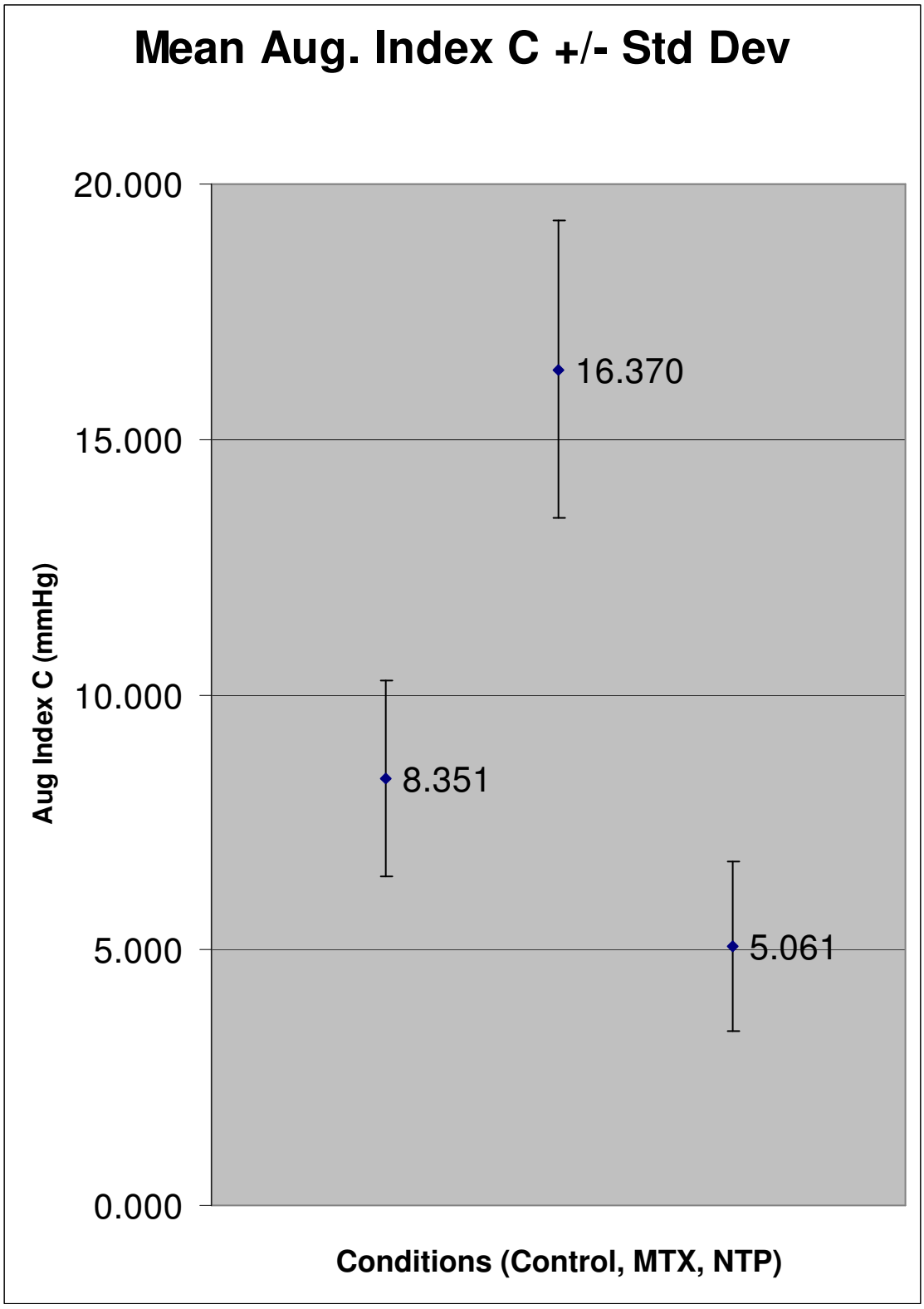

Figure 4.16 - Average Augmentation Index derived by method C (AIC)

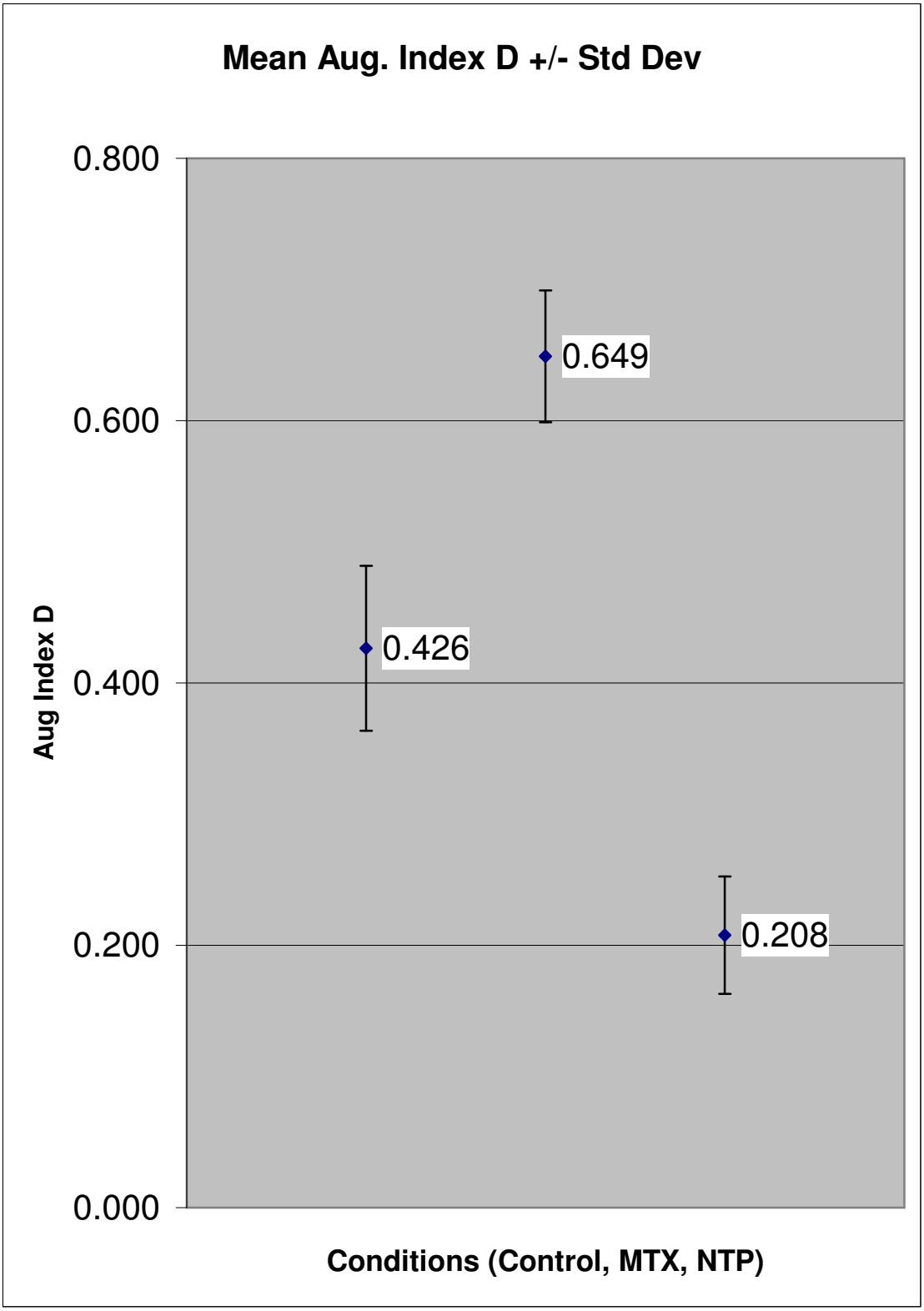

Figure 4.17- Average Augmentation Index derived by method D (AID)

Two statistical tests were performed to compare the augmentation indices. Analysis of variance (ANOVA) was performed for each index group with the null hypothesis that the means for all three conditions are equal. As such, P-value decreases as the statistical distinction between the means increases.

One-tail t-tests were also done comparing the means of induced-hypertension (MTX) and induced vasodilation (NTP) with the mean or the control condition. Again the null hypothesis was that the two means (Control and MTX or NTP) are equal; the alternative hypothesis was that one mean is greater than the other. So again, the P-value decreases as the statistical distinction between the means increases. The average of the two P-one-tail values obtained was also derived.

		Control	MTX	NTP
Set 1	PPf	20.79	26.21	24.82
	PPr	9.76	17.82	4.97
Set 2	PPf	22.02	23.90	23.13
	PPr	7.98	15.36	6.28
Set 4	PPf	15.05	18.49	16.46
	PPr	5.78	12.81	2.75
Set 6	PPf	20.17	33.56	32.50
	PPr	9.89	19.49	6.25

Table 4-2 - Pulse pressure of forward and reflected waves for all datasets

Figure 4.11 shows that the pulse pressure of the forward is essentially independent of the prevailing conditions. The most significant difference is the relative operating pressure – highest for hypertensive state and lowest for vasodilated state. On

the other hand, Figure 4.12 indicates that the pulse pressure of the reflected wave is strongly influenced by the imposed conditions. Table 4.2 summarizes this observation for all four datasets. The pulse pressure of the reflected wave distinctly increases under hypertension and decreases under vasodilation.

Comparison of Augmentation Indices:

AIA and AIC seen in Figures 4.14 and 4.16 respectively possessed regions of overlap. All other indices displayed graphical separation (Figures 4.13, 4.15 and 4.17). However, all except AID showed inconsistencies of their standard deviations (shown as error bars on graphs).

Table 4.1 displays the results of the statistical analysis on the five tested indices. From the P-values generated by ANOVA, the indices would be ranked as follows:

AIB → AID → AIC → Aug → AIA

The P-value of the popular index, AIA, was 0.000881, just under the accepted standard of 0.001for confirmed separation.

While ANOVA considers all three means simultaneously, the t-test can only consider the equality or separation of two means. This test was thus used to illustrate the abilities of the different indices to distinguish 1) induced hypertension from control (normotensive) condition and 2) induced vasodilation from control. The average of the two P-values generated was then used to rank the indices:

AID → Aug → AIB → AIC → AIA

The average P-value of AID for the t-test was 0.000958; that of Aug, the next in rank, was 0.00674.

	Zo - Characteristic Impedance			Rs - Total Peripheral Resistance			Ct - Compliance (Time-domain)		
	Control	MTX	NTP	Control	MTX	NTP	Control	MTX	NTP
	1	2	3	1	2	3	1	2	3
Set 1	0.1724	0.2197	0.1689	4.7173	6.5524	2.9316	0.3632	0.2370	1.4652
Set 2	0.2238	0.1553	0.1402	4.9414	5.2296	2.9516	0.3235	0.2976	1.2550
Set 4	0.1480	0.1407	0.1605	4.7320	5.5211	2.6635	0.4787	0.3797	0.6537
Set 6	0.1705	0.3102	0.2457	4.4610	10.6773	1.8523	0.3614	0.1628	0.6469
Mean	0.1787	0.2065	0.1788	4.7129	6.9951	2.5998	0.3817	0.2693	1.0052
Std Dev	0.0320	0.0772	0.0462	0.1967	2.5195	0.5153	0.0672	0.0920	0.4187
P-value - ANOVA	7.23E-01			7.84E-03			5.14E-03		

Table 4-3 - Analysis of variance of windkessel parameters

	Systolic Pressure			Diastolic Pressure			Mean Aortic Pressure		
	Ctrl	MTX	NTP	Ctrl	MTX	NTP	Control	MTX	NTP
Set 1	132.0	180.0	104.0	105.0	143.9	79.6	117.2	159.9	86.2
Set 2	128.0	164.0	102.4	103.0	132.0	76.0	115.5	146.2	83.7
Set 3	95.0	155.0	68.5	76.0	130.0	50.5	84.0	141.3	57.0
Set 4	105.0	200.0	83.0	80.0	155.0	49.0	90.5	171.3	61.3
Mean	115.0	174.8	89.5	91.0	140.2	63.8	101.8	154.7	72.0
St. Dev	17.87	19.76	16.93	15.12	11.60	16.27	17.04	13.60	15.01
P-one tail t-test		2.08E-03	4.17E-02		1.04E-03	2.49E-02		1.42E-03	1.98E-02
P(t-test) mean		2.19E-02			1.29E-02			1.06E-02	
P-value ANOVA	2.86E-04			1.25E-04			1.05E-04		

Table 4-4 - Statistical analysis of blood pressure values

Table 4.3 illustrates the general changes that occur with induced vasoconstriction (MTX) and vasodilation (NTP). As expected the characteristic impedance remained constant as supported by a p-value of 0.723 for the ANOVA of the three conditions. The peripheral resistance increased with vasoconstriction and decreased with vasodilation in accordance with Poiseuille's law.

Table 4.4 shows that the P-values from ANOVA of the classic markers, systolic and diastolic blood pressure, were less than 0.001, and they were also less than the P-value obtained from ANOVA of augmentation index A.

Chapter 5. Discussion and Future Research

5.1 Compliance Estimation Methods

The collagen and smooth muscle present in arteries impose constraints on the elasticity of the arteries. The tensile strength of collagen, coupled with the tendency of muscles to have increased contractility when stretched, results in the decrease of compliance when arteries are distended under pressure loading. The pressure dependent compliance method allows this changing compliance to be accounted for throughout the cardiac cycle, hence its superiority when incorporated into the windkessel model.

The significant compliance changes demonstrated in this thesis resulted from changes in the arterial muscular tone. The methoxamine used induced vasoconstriction by forcing contraction of the smooth muscles. This resulted in increased peripheral resistance since the lumen diameter was reduced and also in reduced compliance due to the increased muscle tone. The nitroprusside had the opposite effect, since it results in relaxation of the arterial wall muscles. This allowed increased compliance and decreased peripheral resistance.

On the other hand, the compliance and peripheral resistance changes associated with disease induced hypertension cannot be attributed directly to changing muscle tone. The physiological mechanisms that lead to hypertension are not fully understood, especially for primary hypertension.

While the pressure dependent method of compliance estimation continues to be the most robust time domain method, it however receives little use in the general cardiovascular engineering community. The main reason for this would be its complexity

relative to the other methods. The pressure-dependent method involved the use of constants obtained from previous experiments, rather than directly from the pressure and flow data as was the case in the other compliance estimation methods. Thus, with its direct derivation, the time-domain method deserves credit and would be the most suitable method for implementation of hardware based compliance estimations.

5.2 Aortic Pressure-Volume Relation

The compliance-pressure loops from aorta have been shown to be a potential indicator of cardiac health and therapeutic efficacy (Li, 1998b). This thesis attempted to extend on this work to highlight a role for aortic volume-pressure loops based on the pressure dependent compliance.

From the results obtained we see that the average gradient of the volume-pressure curve decreased under hypertensive conditions indicative of the decreased compliance. The hysteresis present was negligible compared to that obtained from the compliance-pressure loops, and as such could not be used to derive conclusions about the cardiac state. As such, no extra information is obtained from this model than was already derived from the compliance-pressure loops. Therefore, further study of the compliance-pressure may be warranted, but the extra calculations to derive the aortic volume changes cannot be justified.

On the other hand, these loops can be compared to simultaneous aortic volume measurements, by ultrasound imaging techniques to test the efficacy of the compliance models. This would lead to further improvement of the models, aiding in the derivation of non-invasive techniques for central pressure measurements.

5.3 Augmentation Index Comparison

The comparison of augmentation indices revealed that the most popular method produced the least significant distinction between the three conditions. However, all methods produced satisfactory ANOVA results ($P < 0.001$) for separation of means in differentiating control from hypertension and subsequent vasodilation.

The proposed augmentation indices, AIB and AID show promise of being robust indicators of arterial reflections that lead to pressure pulse augmentation. Table 5.1 below highlights the key augmentation indices and compares them to the classic diagnostic methods of arterial pressure.

	P-value - t-tests – mean	P-value - ANOVA
Systolic Pressure	2.190E-02	2.864E-04
Diastolic Pressure	1.295E-02	1.246E-04
Mean Aortic Pressure	1.062E-02	1.046E-04
Augmentation Index A	1.588E-02	8.813E-04
Augmentation Index B	8.967E-03	4.574E-07
Augmentation Index D	9.586E-04	3.481E-06

Table 5-1 - Summary of comparison of Augmentation Indices

The table shows that all indices can distinguish between the various conditions, suggesting that the traditional methods should remain in place considering their ease of derivation. However, the experiment used to obtain these results involved high dose vasoconstrictor and vasodilator drugs, as such the separation of the induced conditions from the control levels were drastic. Therefore, the fact that AIB and AID had much

lower P-values, suggests they would be better able to distinguished less marked deviations from control values.

Also of interest to note is that the traditional methods proved superior to AIA in these results. A distinct flaw of inflection pressure methods (Augmentation and AIA) is that they are affected by the rate of travel of the pressure waves. When the return of the reflected wave occurs close to the peak systolic pressure, the augmentation is underestimated, thereby introducing errors. Based on the AIA would be affected by heart rate. Investigators have found AIA to be inversely related to heart rate (Stefanadis et al., 1998; Wilkinson et al., 2000).

5.4 Non-invasive methods

Understandably, consent for non-invasive data collection methods is much easier to obtain especially for research purposes. As such, development of non-invasive methods is one of the critical aims of cardiovascular engineers. The use of transfer functions to generate the aortic pressure (central pressure) wave from non-invasive recordings of pressure wave at peripheral locations such as the radial and brachial arteries is accepted valid by several groups (Karamanoglu et al 1983; Takazawa et al., 1996; Chen et al., 1997; Soderstrom et al. 1999).

Combined with non-invasive techniques for measuring flow, such as ultrasound Doppler, the transfer-function central pressure waveforms would allow the promising analyses demonstrated in this thesis to be performed without the use of catheters or other invasive measurement techniques.

5.5 Future Research

The robustness of the pressure dependent compliance within the three element windkessel has been reiterated. Li et al., in 1990 demonstrated an optimization sequence that further improved the accuracy of this compliance method. Another possible use of this optimization routine is for curve matching to identify prevalent cardiac malignancy. With the aortic valve resistance considered as part of the characteristic impedance, an optimized windkessel with unusually high characteristic impedance would be indicative of aortic valve stenosis.

This thesis and other past works (Li et al., 1986; Simon et al., 1979, 1992; Randall et al., 1984; Safar et al., 1984; Asmar et al., 1988; Berger and Li, 1990) show decreased arterial compliance as being indicative of hypertension. As such, a low compliance optimized windkessel curve match would also indicate hypertension. Likewise, a model with high total peripheral resistance should indicate peripheral arterial occlusive disease (PAOD). Similar application in a four element model would be able to highlight changes in blood viscosity typically due to change of hematocrit levels.

The augmentation indices can be correlated with pulse wave velocities to yield further incite into the state of the arterial system. This would be pertinent since according to Moens-Korteweg's formula the pulse wave velocity is related to compliance, but not to peripheral resistance. The augmentation indices are indicators of wave reflections and as such are related to both compliance and peripheral resistance.

Long term studies of the ability of augmentation indices to predict hypertensive morbidity are proposed and with the employment of non-invasive methods as mentioned earlier, a large population sample should be relatively easy to obtain.

References

1. Asmar, R.G., Pannier, B., Santoni, J., London, G.M., Levy, B.I., and Safar, M.E. Reversion of cardiac hypertrophy and reduced arterial compliance after converting enzyme inhibition in essential hypertension. *Circulation*, 78: 941-950, 1988.
2. Badimon, JJ; Fuster, V; Chesebro, JH, et al. Coronary atherosclerosis: a multifactorial disease. *Circulation*, 87(Suppl):I13–16, 1993.
3. Berger, D.S. and Li, J. K.-J. Temporal relationship between left ventricular and arterial system elastances. *IEEE Trans. Biomed. Eng,* BME-39/; 404-410, 1992.
4. Calder, W.A., III. Scaling of physiological processes in homeothermic animals. *Ann. Rev. Physiol,* 43:301, 1981.
5. Calder, W.A.,III. *Size, Function and Life History.* Dover, New York, 1996.
6. Chen, C.H., Nevo, E. , Fetics, B., Pak, P. H. , Yin, F. C. P. ,Maughan, W. L. & Kass, D. A. Estimation of central aortic pressure waveform by mathematical transformation of radial tonometry pressure. *Circulation,* 95, 1827—1836, 1997.
7. Cox, R.H. and Pace, J.B. Pressure-flow relations in the vessels of the canine aortic arch. *Am. J. Physiol. 228:* 1-10, 1975.
8. Fantin, F., Mattocks, A., Bulpitt, C.J., Banya, W., and Rajkumar, C.Is augmentation index a good measure of vascular stiffness in the elderly? Age and Ageing. Advance Access published on January 1, 2007, DOI 10.1093/ageing/afl115.*Age Ageing* 36: 43-48, 2007
9. Frank, O. Die Grundform des arteriellen Pulses. Z. Biol. 37:483-526, 1899

10. Garrett Jr., Edward H., Ferguson, Robert D. G., Williams, Scott J. [Internet]. Post mortem reconstitution of circulation; 2004 [cited 2008 Nov 22]. Available from http://www.freepatentsonline.com/6824389.html.

11. Guyton, Arthur C. Textbook of medical physiology, Eighth edition. Philadelphia. W.B. Saunders Company.

12. Hales, S. Statical Essays Containing Haemostaticks. London, 1733

13. Holt, J.P., Rhode, E.A., and Kines, H. Ventricular volumes and body weights in mammals. *Am. J. Physiol.* 215:704, 1968.

14. Holt, J.P., Rhode, E.A., Holt, W.W., and Kines, H. Geometric similarity of aorta, venae cavae, and certain of their branches in mammals. *Am. J. Physiol.* 241:R100, 1981.

15. Isles, CG; Walker, LM; Beevers, GD, et al. Mortality in patients of the Glasgow Blood Pressure Clinic. *J Hypertens.* 4:141–56, 1986.

16. Karamanoglu, M. , O'Rourke, M. F. , Avolio, A. P. & Kelly, R. P. An analysis of the relationship between central aortic and peripheral upper limb pressure waves in man. *European Heart Journal,* 14, 160—167, 1993.

17. Klabunde, Richard E. [Internet]. Cardiovascular Pharmacology Concepts; 2008 [cited 2008 Nov 15]. Available from: http://cvpharmacology.com.

18. Lambermont, B.; Gérard, P.; Detry, O.; Kolh, P.; Potty, P.; Defraigne, J. O.; D'Orio, V.; Marcelle, R.. Comparison between Three- and Four-Element Windkessel Models to Characterize Vascular Properties of Pulmonary Circulation. *Archives of Physiology and Biochemistry*, 105.7, 1997.

19. Levick, JR: An Introduction to Cardiovascular Physiology. London: Arnold, 2003.

20. Li John K-J, Cui Ting, Drzewiecki Gary M: A Non-linear Model of the Arterial System Incorporating a Pressure-Dependent Compliance. *IEEE Trans. On Biomedical Eng.* 37:673-678,1990

21. Li John K-J, Zhu Ying: Arterial Compliance and its Pressure Dependence in Hypertension and Vasodilation. *Angiology*, 45:113-117, 1994.

22. Li, J. K.-J. A new approach to the analysis of cardiovascular function: Allometry. In: Drzewiecki, G. and Li, J. K.-J.; eds., *Analysis and Assessment of Cardiovascular Function.* Springer-Verlag, New York, pp. 13-29, 1998.

23. Li, J. K.-J. A new description of arterial function: The compliance pressure loop. *Angiol. J. Vasc. Dis.* 49:543-548, 1998b

24. Li, J.K.-J., Drzewiecki, G., and Wang, P.R. Compliance of the aorta in acute hypertension. *Proc. 7th Intl. Conf. Cardiovasc. Syst. Dyn.* 7:1-3, 1986.

25. Li, J.K-J. *Mammalian Hemodynamics: Wave Transmission Characteristics and Similarity Analysis.* Ph.D. dissertation, Univ. of Pennsylvania, Philadelphia, 1978.

26. Li, John K-J: The Arterial Circulation – Physical Principles and Clinical Applications. New Jersey: Humana Press, 2000.

27. Liu, Z., K. P. Brin, and F. C. P. Yin. Estimation of total arterial compliance: an improved method and evaluation of current methods. *Am. J. Physiol*. 251 (*Heart Circ. Physiol*. 20): H588– H600, 1986.

28. Mahomed, F.A. The physiological and clinical use of the sphygmograph. Medical Times Gazette 1, 62-64. 1872

29. Murgo, J.P., Westerhof, N., Giolma, J.P., and Altobelli, S.A. Aortic input impedance in normal man: relationship to pressure waveforms. Circu*lation* 62: 105-116, 1980.

30. Murgo, J.P., Westerhof, N., Giolma, J.P., and Altobelli, S.A. Manipulation of ascending aortic pressure and flow wave reflections with the Valsalva maneuver: relationship to input impedance. *Circulation* 63: 122-132, 1981.

31. O'Rourke, M.F. and Gallagher, D.E. Pulse wave analysis. *Journal of Hypertension.* 14:147-157, 1996.

32. Quick, C.M., Li, J.K.-J., O'Hara, D., and Noordergraaf, A. Reconciliation of windkessel and distributed description of linear arterial system. Proc. 1st Summer Bioeng. Conf. 29:469-470, 1995.

33. Randall, O.S., van den Bos, G.C., and Westerhof, N. Systemic compliance: Does it play a role in the genesis of essential hypertension? Cardiovasc. Res. 18:455-462, 1984.

34. Remington, J.W., C.B. Nobach, W.F. Hamilton, and J.J. Gold. Volume elasticity characteristics of the human aorta and the prediction of stroke volume from the pressure pulse. Am. J. Phys. 153: 198-308, 1948.

35. Safar, M.E., Simon, A.C., and Levenson, J.A. Structural changes of larges arteries in sustained essential hypertension. Hypertension. 6(SIII):117-121, 1984.

36. Sierra, Cristina; De La Sierra, Alejandro. Early detection and management of the high-risk patient with elevated blood pressure. Vasc Health Risk Manag. 2008 April; 4(2): 289–296. (Published online 2008 April.)

37. Simon, A.C., Levenson, J.A., Chau, N.P., Pithois-Merli, I. Role of arterial compliance in the physiopharmacological approach to human hypertension. J. Cardiovasc. Pharmacol. 19(S5):11-20, 1992.

38. Simon, A.C., Safar, M.E., Levenson JA, London GM, Levy BI, Chau NP: An evaluation of large arteries compliance in man. Am. J. Physiol. 237:H550-554, 1979.

39. Smith, Ronald D., Levy, Pavel J. Review: New techniques for assessment of vascular function. Therapeutic Advances in Cardiovascular Disease 2008 2: 373-385.

40. Soderstrom, S., Nyberg, G. , Ponten, J. , Sellgren, J. & O'Rourke, M. (1998). Substantial equivalence between ascending aortic pressure waveforms and waveforms derived from the radial pulse using a generalized transfer function? FASEB Journal A712, 4131.

41. Spengler, L. Symbolae and theoriam de sanguinis arteriosi fluimine. Dissertation, Univ. of Marburg, Marburg, 1843.

42. Stahl, W.R. Organ weights in primates and other mammals. *Science* 150:1039-1042, 1965.

43. Stahl, W.R. Similarity analysis of biological systems. *Persp. Biol. Med.* 6:291, 1963.

44. Stefanadis, C., Dernellis, J., Vavuranakis, M., Tsiamis, E., Vlachopoulos, C., Toutouzas, K., Diamandopoulos, L., Pitsavos, C., and Toutouzas, P. Effects of ventricular pacing-induced tachycardia on aortic mechanics in man. *Cardiovascular Research,* 39:506-514, 1998.

45. Takazawa, K. , O'Rourke, M. & Fujita, M. (1996). Estimation of ascending aortic pressure from radial arterial pressure using a generalized transfer function. Zeitschrift fur Kardiologie 85, 137—139.

46. Ting, C., Yang, T., Chen, J., Chen, M.,and Yin, F.C.P. Arterial hemodynamics in human hypertension. Effects of angiotensin converting enzyme inhibitors. Hypertension 22:839-846, 1993.

47. Van Den Bos, G.C., Westerhof, N., Eizinga, G., and Sipkema, P. Reflection in the systemic arterial system: effects of aortic and carotid occlusion. *Cardiovasc. Res. 10:* 565-573, 1976.

48. Von Kries, J. *Studien zur Pulslehre.* Akad. Verlag, Freiberg, 1892.

49. Wang, P.R., Li, J.K.-J., and Drzewiecki, G. Aortic compliance during acute pressure loading. Proc. 39th Ann. Conf. Eng. Med. Biol. 28:246, 1986.

50. Westerhof, N., Bosman, F., DeVries, C.J., and Noordergraaf, A. Analog studies of the human systemic arterial tree. *J. Biomech.* 2: 121-143, 1969.

51. Westerhof, N., Eizinga, G., and Van den Bos, G.C. Influence of central and peripheral changes on the hydraulic input impedance of the systemic arterial tree. *Med. Biol. Eng.* 11:710-723, 1973.

52. Wilkinson, I.B., MacCallum, H., Flint, L., Cockcroft, J.R., Newby, D.E., and Webb, D.J. The influence of heart rate on augmentation index and central arterial pressure in humans. *J. Physiology.* 525.1:263-270, 2000.

53. Zamir, Mair. The Physics of Pulsatile Flow. New York. Springer-Verlag 2000

Appendix I – MATLAB code

This is the general code used to derive the calculated pressure and volume by iterative discrete calculations.

```
clear all;
% ********** Data Import *************

% Load data values into MATLAB - Time (sec), Pressure (mmHg), Flow
(ml/sec)
DataID = textread('C:\Research\datasets\set6\id.txt','%s')

% Control Data -
[t_control, P_control, Q_control] =
textread('C:\Research\datasets\set6\control.txt','%f %f %f');
t_control = t_control';P_control = P_control';Q_control = Q_control';
%figure(1); subplot(2,1,1); plot(t_control, P_control); subplot(2,1,2);
plot(t_control, Q_control);


% MTX6 (induced hypertension) data -
[t_mtx, P_mtx, Q_mtx] =
textread('C:\Research\datasets\set6\mtx.txt','%f %f %f');
t_mtx = t_mtx';P_mtx = P_mtx';Q_mtx = Q_mtx';
%figure(2); subplot(2,1,1); plot(t_mtx, P_mtx); subplot(2,1,2);
plot(t_mtx, Q_mtx);


% NTP6 (induced hypotension) data -
[t_ntp, P_ntp, Q_ntp] =
textread('C:\Research\datasets\set6\ntp.txt','%f %f %f');
t_ntp = t_ntp';P_ntp = P_ntp';Q_ntp = Q_ntp';
%figure(3); subplot(2,1,1); plot(t_ntp, P_ntp); subplot(2,1,2);
plot(t_ntp, Q_ntp);



% ******** Parameter Input**********
% Parameters determined in Excel spreadsheet - (Dataset_ with
parameters)

%Control
Zmean_con = .1705;            %Characteristic Impedance
Rs_con = 4.4610;              %Peripheral Impedance
Ct_con = .3614;               %Compliance - Decay curve method
Cv_con = .3488;               %Compliance - SV/PP method
a_con = 1.2;                        %Parameter's a and b for pressure
dependent compliance
b_con = .01327;


%MTX
Zmean_mtx = .3102;
```

```
Rs_mtx = 10.6773;
Ct_mtx = .1628;
Cv_mtx = .1604;
a_mtx = .825;
b_mtx = .00947;


%NTP
Zmean_ntp = .2457;
Rs_ntp = 1.8523;
Ct_ntp = 0.6469;
Cv_ntp = .3506;
a_ntp = 2.5;
b_ntp = .02204;



%Control
% Error calculation - manually varying a and b - see log book
%Pressure from Cp - pressure dependent compliance
dt = t_control(2) - t_control(1);
for i = 1:(length(t_control)-1);
      Pres_pred_contp(1) = P_control(1);
      Pres_pred_contp(i+1) = Pres_pred_contp(i) +...
         dt * (Q_control(i) - (Pres_pred_contp(i)/Rs_con))/(a_con*exp(-
b_con*(Pres_pred_contp(i))));
end
  Pres_pred_contp = Pres_pred_contp + (Q_control*Zmean_con);
  for i = 1:(length(t_control));
  Error(i) = (((Pres_pred_contp(i) - P_control(i))^2));
end
  E_controlp = sqrt(sum(Error));

Ep = strcat('Calc. Pres. by Cp, Ep=',(num2str(E_controlp,4))); %create
label string for graph legend

%Pressure from Ct - time-decay method for compliance determination
for i = 1:(length(t_control)-1);
      Pres_pred_contt(1) = P_control(1);
      Pres_pred_contt(i+1) = Pres_pred_contt(i) +...
         dt * (Q_control(i) - (Pres_pred_contt(i)/Rs_con))/(Ct_con);
end
  Pres_pred_contt = Pres_pred_contt + (Q_control*Zmean_con);
  for i = 1:(length(t_control));
  Error(i) = (((Pres_pred_contt(i) - P_control(i))^2));
end
  E_controlt = sqrt(sum(Error));

Et = strcat('Calc. Pres. by Ct, Et=',(num2str(E_controlt,4))); %create
label string for graph legend


%Pressure from Cv - time-decay method for compliance determination
for i = 1:(length(t_control)-1);
      Pres_pred_contv(1) = P_control(1);
      Pres_pred_contv(i+1) = Pres_pred_contv(i) +...
         dt * (Q_control(i) - (Pres_pred_contv(i)/Rs_con))/(Cv_con);
```

```
end
  Pres_pred_contv = Pres_pred_contv + (Q_control*Zmean_con);
  for i = 1:(length(t_control));
  Error(i) = (((Pres_pred_contv(i) - P_control(i))^2));
end
  E_controlv = sqrt(sum(Error));

Ev = strcat('Calc. Pres. by Cv, Ev=',(num2str(E_controlv,4))); %create
label string for graph legend

%Make graph title string
head = strcat('Aortic Pressure (meas. & calc.) and Flow Waveforms under
Control Condition -  ',DataID);

figure(4);
subplot(2,1,1);plot(t_control, P_control,'k');hold on;
subplot(2,1,1);plot(t_control,Pres_pred_contp,'b-.');
subplot(2,1,1);plot(t_control,Pres_pred_contt,'g--');
subplot(2,1,1);plot(t_control,Pres_pred_contv,'r:');hold off;
title(head);
xlabel('Time (seconds)');ylabel('Pressure (mmHg)');legend('Measured
Pressure',Ep,Et,Ev);
subplot(2,1,2);plot(t_control, Q_control);
xlabel('Time (seconds)');ylabel('Flow (mL)');



%MTX - Hypertension
% Error calculation - manually varying a and b - see log book
%Pressure from Cp - pressure dependent compliance
dt = t_mtx(2) - t_mtx(1);
for i = 1:(length(t_mtx)-1);
      Pres_pred_mtxp(1) = P_mtx(1);
      Pres_pred_mtxp(i+1) = Pres_pred_mtxp(i) +...
         dt * (Q_mtx(i) - (Pres_pred_mtxp(i)/Rs_mtx))/(a_mtx*exp(-
b_mtx*(Pres_pred_mtxp(i))));
end
Pres_pred_mtxp = Pres_pred_mtxp + (Q_mtx*Zmean_mtx);

for i = 1:(length(t_mtx));
   Errorp(i) = (((Pres_pred_mtxp(i) - P_mtx(i))^2));
end
E_mtxp = sqrt(sum(Errorp));

Emtxp = strcat('Calc. Pres. by Cp, Ep=',(num2str(E_mtxp,4))); %create
label string for graph legend


%Pressure from Ct - time-decay method for compliance determination
for i = 1:(length(t_mtx)-1);
      Pres_pred_mtxt(1) = P_mtx(1);
      Pres_pred_mtxt(i+1) = Pres_pred_mtxt(i) +...
         dt * (Q_mtx(i) - (Pres_pred_mtxt(i)/Rs_mtx))/(Ct_mtx);
end
  Pres_pred_mtxt = Pres_pred_mtxt + (Q_mtx*Zmean_mtx);
  for i = 1:(length(t_mtx));
```

```
  Errort(i) = (((Pres_pred_mtxt(i) - P_mtx(i))^2));
end
  E_mtxt = sqrt(sum(Errort));

Emtxt = strcat('Calc. Pres. by Ct, Et=',(num2str(E_mtxt,4))); %create
label string for graph legend


%Pressure from Cv - stroke volume method for compliance determination;
for i = 1:(length(t_mtx)-1);
      Pres_pred_mtxv(1) = P_mtx(1);
      Pres_pred_mtxv(i+1) = Pres_pred_mtxv(i) +...
         dt * (Q_mtx(i) - (Pres_pred_mtxv(i)/Rs_mtx))/(Cv_mtx);
end
  Pres_pred_mtxv = Pres_pred_mtxv + (Q_mtx*Zmean_mtx);
  for i = 1:(length(t_mtx));
  Errorv(i) = (((Pres_pred_mtxv(i) - P_mtx(i))^2));
end
  E_mtxv = sqrt(sum(Errort));

Emtxv = strcat('Calc. Pres. by Cv, Ev=',(num2str(E_mtxv,4))); %create
label string for graph legend


%Make graph title string
headmtx = strcat('Aortic Pressure and Flow Waveforms under Methoxamine
induced Hypertension -  ',DataID);

figure(5);;
subplot(2,1,1);plot(t_mtx, P_mtx,'k');hold on;
subplot(2,1,1);plot(t_mtx,Pres_pred_mtxp,'b-.');
subplot(2,1,1);plot(t_mtx,Pres_pred_mtxt,'g--');
subplot(2,1,1);plot(t_mtx,Pres_pred_mtxv,'r:');hold off;
title(headmtx);
xlabel('Time (seconds)');ylabel('Pressure (mmHg)');legend('Measured
Pressure',Emtxp,Emtxt,Emtxv);
subplot(2,1,2);plot(t_mtx, Q_mtx);
xlabel('Time (seconds)');ylabel('Flow (mL)');



%NTP - Hypotension
% Error calculation - manually varying a and b - see log book
dt = t_ntp(2) - t_ntp(1);
for i = 1:(length(t_ntp)-1);
      Pres_pred_ntpp(1) = P_ntp(1);
      Pres_pred_ntpp(i+1) = Pres_pred_ntpp(i) +...
         dt * (Q_ntp(i) - (Pres_pred_ntpp(i)/Rs_ntp))/(a_ntp*exp(-
b_ntp*(Pres_pred_ntpp(i))));
end
  Pres_pred_ntpp = Pres_pred_ntpp + (Q_ntp*Zmean_ntp);
  for i = 1:(length(t_ntp));
  Error_ntpp(i) = (((Pres_pred_ntpp(i) - P_ntp(i))^2));
end
  E_ntpp = sqrt(sum(Error_ntpp));
```

```
Entpp = strcat('Calc. Pres. by Cp, Ep=',(num2str(E_ntpp,4))); %create
label string for graph legend


%Pressure from Ct - time-decay method for compliance determination
for i = 1:(length(t_ntp)-1);
      Pres_pred_ntpt(1) = P_ntp(1);
      Pres_pred_ntpt(i+1) = Pres_pred_ntpt(i) +...
         dt * (Q_ntp(i) - (Pres_pred_ntpt(i)/Rs_ntp))/(Ct_ntp);
end
  Pres_pred_ntpt = Pres_pred_ntpt + (Q_ntp*Zmean_ntp);
  for i = 1:(length(t_ntp));
  Error_ntpt(i) = (((Pres_pred_ntpt(i) - P_ntp(i))^2));
end
  E_ntpt = sqrt(sum(Error_ntpt));

Entpt = strcat('Calc. Pres. by Ct, Et=',(num2str(E_ntpt,4))); %create
label string for graph legend


%Pressure from Cv - SV method for compliance determination
for i = 1:(length(t_ntp)-1);
      Pres_pred_ntpv(1) = P_ntp(1);
      Pres_pred_ntpv(i+1) = Pres_pred_ntpv(i) +...
         dt * (Q_ntp(i) - (Pres_pred_ntpv(i)/Rs_ntp))/(Cv_ntp);
end
  Pres_pred_ntpv = Pres_pred_ntpv + (Q_ntp*Zmean_ntp);
  for i = 1:(length(t_ntp));
  Error_ntpv(i) = (((Pres_pred_ntpv(i) - P_ntp(i))^2));
end
  E_ntpv = sqrt(sum(Error_ntpv));

Entpv = strcat('Calc. Pres. by Cv, Ev=',(num2str(E_ntpv,4))); %create
label string for graph legend


%Make graph title string
headntpv = strcat('Aortic Pressure and Flow Waveforms under
Nitroprusside induced Hypotension -  ',DataID);

figure(6);
subplot(2,1,1);plot(t_ntp, P_ntp,'k');hold on;
subplot(2,1,1);plot(t_ntp,Pres_pred_ntpp,'b-.');
subplot(2,1,1);plot(t_ntp,Pres_pred_ntpt,'g--');
subplot(2,1,1);plot(t_ntp,Pres_pred_ntpv,'r:');hold off;
title(headntpv);
xlabel('Time (seconds)');ylabel('Pressure (mmHg)');legend('Measured
Pressure',Entpp,Entpt,Entpv);
subplot(2,1,2);plot(t_ntp, Q_ntp);
xlabel('Time (seconds)');ylabel('Flow (mL)');



figure(7);
plotyy(P_control,Q_control,Pres_pred_contp,Q_control);
figure(8);
plotyy(P_mtx,Q_mtx,Pres_pred_mtxp,Q_mtx);
```

```
figure(9);
plotyy(P_ntp,Q_ntp,Pres_pred_ntpp,Q_ntp);

figure(10);hold on;
plot(Pres_pred_contp,Q_control,'r');
plot(Pres_pred_mtxp,Q_mtx,'k:');
plot(Pres_pred_ntpp,Q_ntp,'b-.');
title('Comparison of Pressure-Flow Loops for the three investigated
conditions');
xlabel('Predicted Aortic Pressure (mmHg)'); ylabel('Measured Flow
(mL/sec)');
legend('Control','MTX','NTP');text(0,0,DataID);
hold off;


%Control
dt = t_control(2) - t_control(1);
for i = 1:(length(Q_control)-1);
   SV_cont(i) = dt * ((Q_control(i+1)+Q_control(i)))/2;
end
SV_control = sum(SV_cont)

%Methoxamine
dt = t_mtx(2) - t_mtx(1);
for i = 1:(length(Q_mtx)-1);
   SV_metx(i) = dt * ((Q_mtx(i+1)+Q_mtx(i)))/2;
end
SV_mtx = sum(SV_metx)

%Nitroprusside
dt = t_ntp(2) - t_ntp(1);
for i = 1:(length(Q_ntp)-1);
   SV_nitp(i) = dt * ((Q_ntp(i+1)+Q_ntp(i)))/2;
end
SV_ntp = sum(SV_nitp)


%Control
%V_cont(1) = SV_control;
V_cont(1) = 0;
for i = 1:(length(Pres_pred_contp)-1);
   V_cont(i+1) = V_cont(i) + (Pres_pred_contp(i+1)-Pres_pred_contp(i))
* a_con * exp(-b_con*Pres_pred_contp(i));
end



%Methoxamine
%V_mtx(1) = SV_mtx;
V_mtx(1) = 0;
for i = 1:(length(Pres_pred_mtxp)-1);
   V_mtx(i+1) = V_mtx(i) + (Pres_pred_mtxp(i+1)-Pres_pred_mtxp(i)) *
a_mtx * exp(-b_mtx*Pres_pred_mtxp(i));
end


%Nitroprusside
```

```
%V_ntp(1) = SV_ntp;
V_ntp(1) = 0;
for i = 1:(length(Pres_pred_ntpp)-1);
   V_ntp(i+1) = V_ntp(i) + (Pres_pred_ntpp(i+1)-Pres_pred_ntpp(i)) *
a_ntp * exp(-b_ntp*Pres_pred_ntpp(i));
end

figure(11);
plot(Pres_pred_contp,V_cont,'r');
title('Predicted Pressure-Volume(dV) Curve for Control Condition');
xlabel('Calculated Aortic Pressure (mmHg)');ylabel('Calculated Aortic
Volume Change (mL)');
figure(12);
plot(Pres_pred_mtxp,V_mtx,'k');
title('Predicted Pressure-Volume(dV) Curve for Methoxamine Induced
Hypertensive Condition');
xlabel('Calculated Aortic Pressure (mmHg)');ylabel('Calculated Aortic
Volume Change (mL)');
figure(13);
plot(Pres_pred_ntpp, V_ntp,'b');
title('Predicted Pressure-Volume(dV) Curve for Nitroprusside Induced
Hypotensive Condition');
xlabel('Calculated Aortic Pressure (mmHg)');ylabel('Calculated Aortic
Volume Change (mL)');

figure(14);hold on;
plot(Pres_pred_contp,V_cont,'r');
plot(Pres_pred_mtxp,V_mtx,'k:');
plot(Pres_pred_ntpp, V_ntp,'b-.');
title('Predicted Pressure-Volume(dV) Curve comparing all three
conditions');
xlabel('Calculated Aortic Pressure (mmHg)');ylabel('Calculated Aortic
Volume Change (mL)');
legend('Control','Hypertension','Hypotension');
hold off;

figure(15);hold on;
plot(Q_control,V_cont,'r');
plot(Q_mtx,V_mtx,'k:');
plot(Q_ntp, V_ntp,'b-.');
title('Calculated Volume Change vs Measured Flow Curve comparing all
three conditions');
xlabel('Measured Aortic Flow (mL)');ylabel('Calculated Aortic Volume
Change (mL)');
legend('Control','Hypertension','Hypotension');
hold off;

figure(16);hold on;
plot(t_control,V_cont,'r');
title('Time curve of the calculated Aorta Volume for all three
conditions');
xlabel('Time (seconds)'); ylabel('Calculated Aorta Volume');
plot(t_mtx,V_mtx,'k:');
plot(t_ntp,V_ntp,'b-.');legend('Control','MTX - Hypertension','NTP -
Hypotension')
hold off;
```